MICROCOPY RESOLUTION TEST CHART

NATIONAL BUREAU OF STANDARDS-1963-A

②

UCLA School of Engineering and Applied Science

"Criteria for Nearly Omnidirectional Radiation Patterns for Printed Antennas"

By N. G. Alexopoulos, D. R. Jackson, and P. B. Katehi

Integrated Electromagnetics Laboratory
Report No. 12
UCLA Report No. ENG-84-18
May 31, 1984

DTIC
ELECTE
JUL 27 1984

B

REPORT DOCUMENTATION PAGE		READ INSTRUCTIONS BEFORE COMPLETING FORM
1. REPORT NUMBER ARO 19778.4-EL	2. GOVT ACCESSION NO.	3. RECIPIENT'S CATALOG NUMBER
4. TITLE (and Subtitle) "Criteria for Nearly Omnidirectional Radiation Patterns for Printed Antennas"		5. TYPE OF REPORT & PERIOD COVERED
		6. PERFORMING ORG. REPORT NUMBER
7. AUTHOR(s) N. G. Alexopoulos, D.R. Jackson, and P.B. Katehi		8. CONTRACT OR GRANT NUMBER(s) Northrop Corp. 82-110-1006 U.S.Army DAAG 29-83-K-0067
9. PERFORMING ORGANIZATION NAME AND ADDRESS Electrical Engineering Department UCLA Los Angeles, CA 90024		10. PROGRAM ELEMENT, PROJECT, TASK AREA & WORK UNIT NUMBERS
11. CONTROLLING OFFICE NAME AND ADDRESS U. S. Army Research Office Post Office Box 12211 Research Triangle Park, NC 27709		12. REPORT DATE May 31, 1984
		13. NUMBER OF PAGES
14. MONITORING AGENCY NAME & ADDRESS(If different from Controlling Office) Army Research Office Northrop Corporation Research Triangle Park North Carolina		15. SECURITY CLASS. (of this report) Unclassified
		15a. DECLASSIFICATION/DOWNGRADING SCHEDULE

16. DISTRIBUTION STATEMENT (of this Report)

Approved for public release; distribution unlimited.

17. DISTRIBUTION STATEMENT (of the abstract entered in Block 20, If different from Report)

NA

18. SUPPLEMENTARY NOTES

The view, opinions, and/or findings contained in this report are those of the author(s) and should not be construed as an official Department of the Army position, policy, or decision, unless so designated by other documentation.

19. KEY WORDS (Continue on reverse side If necessary and identify by block number)

20. ABSTRACT (Continue on reverse side If necessary and identify by block number)

Radiation from printed antennas is investigated with emphasis placed on producing E- and H-plane radiation patterns which are as nearly omnidirectional as possible. This is achieved using criteria which are derived for a nonzero radiation field extending down to the layer surface (radiation into the horizon). It is determined that this phenomenon arises when a surface wave pole coincides with a branch point in the complex plane. A simple ray optics interpretation is given for a phenomenon, and graphs are presented to easily enable design of printed antenna geometry to achieve nearly omnidirectional E- or H-plane patterns.

DD FORM 1473 EDITION OF 1 NOV 65 IS OBSOLETE

CRITERIA FOR NEARLY OMNIDIRECTIONAL RADIATION
PATTERNS FOR PRINTED ANTENNAS

BY

N. G. Alexopoulos, D. R. Jackson, and P. B. Katehi
Electrical Engineering Department
University of California Los Angeles
Los Angeles, California   90024

ABSTRACT

Radiation from printed antennas is investigated with emphasis placed on producing $\overline{E}$- and $\overline{H}$-plane radiation patterns which are as nearly omnidirectional as possible. This is achieved using criteria which are derived for a nonzero radiation field extending down to the layer surface (radiation into the horizon). It is determined that this phenomenon arises when a surface wave pole coincides with a branch point in the complex plane. A simple ray optics interpretation is given for the phenomenon, and graphs are presented to easily enable design of printed antenna geometry to achieve nearly omnidirectional $\overline{E}$- or $\overline{H}$-plane patterns.

I. INTRODUCTION

Investigation of printed circuit antennas and associated substrate effects [1]-[9] has uncovered certain interesting phenomena. One such phenomenon is the existence of nonzero radiation along the horizon in either the $\overline{E}$- or the $\overline{H}$-plane when the electrical thickness of the substrate satisfies specific criteria. In particular, $\overline{H}$-plane radiation into the horizon is seen to occur when a TE surface wave mode turns on in the substrate, and $\overline{E}$-plane radiation into the horizon can be observed when a TM mode turns on. This phenomenon is explained analytically by the coincidence of a pole and a branch point in a Sommerfeld-type integration, which gives rise to a removable singularity in the steepest descent integration for the far-field. A ray optics interpretation is given to aid in the physical understanding of the phenomenon. Criteria are then determined for optimum antenna location within a substrate to yield $\overline{E}$- or $\overline{H}$-plane patterns as omnidirectional as possible in a specified sense. Based on this, graphs are presented enabling design of proper substrate-antenna geometry to achieve nearly omnidirectional radiation patterns. These results are then extended to the more general case of a dipole printed on a substrate with a different superstrate (cover) material on top.

Although the problem discussed herein is akin to a large number of investigations in the propagation of electromagnetic waves in stratified media [10]-[14], the thrust of this paper is the unique observation of radiation into the horizon and the generation of nearly omnidirectional radiation patterns.

II. RADIATION INTO THE HORIZON

With reference to Figure 1a, the problem consists in its simplest form of a horizontal infinitesimal dipole in the $\hat{x}$ direction embedded inside a grounded substrate layer. The results which pertain to this configuration can be generalized to the case of a dipole in a substrate-superstrate configura-

tion of different materials, shown in Figure 1b. However, in order to high-light the criteria under which radiation into the horizon takes place and to keep the mathematical complexities to a minimum, the case of Figure 1a will be considered in detail, with only results shown for the more general case of Figure 1b.

The far-field due to the elementary horizontal dipole at $z = z_o$ in a substrate of thickness B, relative permittivity and permeability constants ϵ_1, μ_1 and index of refraction $n_1 = \sqrt{\epsilon_1 \mu_1}$, is given in spherical coordinates by [2], [5]

$$E_\theta \sim k_o^2 [\cos\theta\cos\phi \Pi_x - \sin\theta \Pi_z]$$ (1)

and

$$E_\phi \sim k_o^2 [-\sin\phi \Pi_x] .$$ (2)

In these equations $k_o = \omega\sqrt{\mu_o \epsilon_o}$, ϵ_o and μ_o being the total permittivity and permeability of free space.

The Hertz potential components Π_x, Π_z for $z > B$ are given in cylindrical coordinates as [2], [5] (suppressing $e^{+j\omega t}$ time dependence)

$$\Pi_x = \frac{-j\omega\mu_o}{8\pi k_1^2} \int_{-\infty}^{+\infty} \frac{f(\lambda)}{D_e(\lambda)} e^{-u(z-B)} H_o^{(2)}(\lambda r) d\lambda$$ (3)

and

$$\Pi_z = \frac{-j\omega\mu_o}{8\pi k_1^2} \cos\phi \int_{-\infty}^{+\infty} \frac{g(\lambda)}{D_e(\lambda) D_m(\lambda)} e^{-u(z-B)} H_1^{(2)}(\lambda r) d\lambda$$ (4)

where $k_1 = k_o n_1$ and

$$f(\lambda) = 2\lambda n_1^2 \sinh(u_1 z_o)$$ (5)

$$g(\lambda) = 2\lambda^2 (1-n_1^2) n_1^2 \cosh(u_1 B) \sinh(u_1 z_o)$$ (6)

$$D_e(\lambda) = \mu_1 u \sinh(u_1 B) + u_1 \cosh(u_1 B)$$ (7)

-2-

$$D_m(\lambda) = un_1^2\cosh(u_1 B) + \mu_1 u_1 \sinh(u_1 B) \tag{8}$$

with
$$u = (\lambda^2 - k_o^2)^{1/2} \quad, \quad u_1 = (\lambda^2 - k_1^2)^{1/2} \quad. \tag{9}$$

The branch interpretation of u is $u = \left|(\lambda^2 - k_o^2)^{1/2}\right|$ for $\lambda \geq k_o$ and $u = j\left|(\lambda^2 - k_o^2)^{1/2}\right|$ for $\lambda \leq k_o$. The branch interpretation of u_1 is arbitrary.

The Sommerfeld contour inferred by Equations (3), (4) is shown in Figure 2a. If the substitutions $\lambda = k_o\sin\zeta$, $z - B = R\cos\theta$, $r = R\sin\theta$ are intro-duced (where R and θ describe spherical coordinates) together with the large argument asymptotic expansions for $H_o^{(2)}(\lambda r)$ and $H_1^{(2)}(\lambda r)$, Equations (3) and (4) can be written as

$$\Pi_x = \frac{1}{\sqrt{k_o R}} \int_\Gamma F(\zeta) e^{\Omega h(\zeta)} d\zeta \tag{10}$$

and
$$\Pi_z = \frac{\cos\phi}{\sqrt{k_o R}} \int_\Gamma G(\zeta) e^{\Omega h(\zeta)} d\zeta \tag{11}$$

where Γ is the path shown in Figure 2b which can be deformed into the steepest descent path (S.D.P.) also shown there, and

$$\Omega = k_o R \quad, \quad h(\zeta) = -j\cos(\zeta-\theta)$$

$$F(\zeta) = \frac{(k_o\cos\zeta)\, f(k_o\sin\zeta)}{D_e(k_o\sin\zeta)} \left(\frac{-j\omega\mu_o}{8\pi k_1^2} \frac{(1+j)}{\sqrt{\pi\sin\theta\sin\zeta}}\right) \tag{12}$$

$$G(\zeta) = \frac{(k_o\cos\zeta)\, g(k_o\sin\zeta)}{D_e(k_o\sin\zeta)\, D_m(k_o\sin\zeta)} \left(\frac{-j\omega\mu_o}{8\pi k_1^2} \frac{j(1+j)}{\sqrt{\pi\sin\theta\sin\zeta}}\right) \quad. \tag{13}$$

The saddle point is at $\zeta = \zeta_o = \theta$, and the departure angle from the saddle point is $\alpha = +\frac{\pi}{4}$. The roots of $D_e(\lambda)$ and $D_m(\lambda)$ give surface wave poles whose residue contributions determine the TE and TM mode surface waves respectively [2], [5]. The steepest descent path is deformed to go around the poles as shown in Figure 2b. However, due to the exponential decay away from the saddle point along the steepest descent path, the residue contributions from these poles

do not contribute to the asymptotic expansions of Π_x and Π_z unless $\theta = \pi/2$.
For this latter case, the contour of integration can be broken into two parts:
a steepest descent contour and an integration around the poles, as shown in
Figure 2c. The surface wave fields, determined by the integration around the
poles, contribute at $\theta = \pi/2$ since we are in the vicinity of the layer material.
These surface wave fields remain distinct from the steepest descent contribu-
tion, however, which gives the radiated far-field which is of interest here.

The method of steepest descents now yields

$$\Pi_x \sim F(\theta) \sqrt{2\pi} \, e^{j\frac{\pi}{4}} \left(\frac{e^{-jk_oR}}{k_oR} \right) \tag{14}$$

and

$$\Pi_z \sim \cos\phi \, G(\theta) \sqrt{2\pi} \, e^{j\frac{\pi}{4}} \left(\frac{e^{-jk_oR}}{k_oR} \right) \quad . \tag{15}$$

Equations (1), (2), (12), (13) are combined with (14) and (15) to give
the far-field of the dipole. The far-field clearly decays as $1/k_oR$ for $k_oR \gg 1$.
For convenience, the radiated field is defined so as to suppress this radial
dependence, i.e.

$$E_\theta \sim \frac{E_\theta^R}{k_oR} e^{-jk_oR} \tag{16}$$

and

$$E_\phi \sim \frac{E_\phi^R}{k_oR} e^{-jk_oR} \tag{17}$$

where, by definition,

$$E_\theta^R = k_o^2 [\cos\theta\cos\phi \Pi_x^R - \sin\theta \Pi_z^R] \tag{18}$$

$$E_\phi^R = k_o^2 [-\sin\phi \Pi_x^R] \tag{19}$$

and

$$\Pi_x^R = \lim_{k_oR \to \infty} (k_oR) \, e^{+jk_oR} \Pi_x \tag{20}$$

-4-

$$\Pi_z^R = \lim_{k_o R \to \infty} (k_o R) \, e^{+jk_o R} \, \Pi_z \, . \tag{21}$$

E_θ^R and E_ϕ^R are functions of θ and ϕ only. The variation of the radiation field with θ is governed by the $F(\theta)$ and $G(\theta)$ functions. With reference to Equations (12) and (13), it is observed that a factor $\cos\theta$ appears in both $F(\theta)$ and $G(\theta)$. This implies that in general,

$$\lim_{\theta \to \pi/2} \Pi_{x,z}^R = 0 \tag{22}$$

and   therefore

$$\lim_{\theta \to \pi/2} E_\theta^R = 0 \tag{23}$$

and

$$\lim_{\theta \to \pi/2} E_\phi^R = 0 \, . \tag{24}$$

That is, the radiated field tends to zero at the horizon ($\theta \to \pi/2$). The only possible exception is when the terms $D_e(k_o \sin\theta)$ or $D_m(k_o \sin\theta)$ also tend to zero as $\theta \to \pi/2$. When $D_e(k_o) = 0$, it follows from Eq. (7) that

$$\left(\frac{n_1 B}{\lambda_o}\right)\sqrt{1 - 1/n_1^2} = (m - 1/2)/2, \tag{25}$$
$$m = 1,2,\ldots$$

while when $D_m(k_o) = 0$, then from Eq. (8)

$$\left(\frac{n_1 B}{\lambda_o}\right)\sqrt{1 - 1/n_1^2} = (m-1)/2, \tag{26}$$
$$m = 1,2,\ldots$$

is obtained, where λ_o = free-space wavelength.

Equations (25) and (26) are simply the conditions for a TE and a TM surface wave mode turning on, respectively.

The characteristic functions $D_e(\lambda)$ and $D_m(\lambda)$ have simple zeros at the location of the surface wave poles in the complex λ-plane except when a pole

coincides exactly with the branch point at $\lambda = k_o$, which occurs when the corresponding surface wave mode turns on. In this case, the function $D_e(\lambda)$ or $D_m(\lambda)$ exhibits a branch point type of singularity there. In particular, as $\lambda \to k_o$

$$D_e(\lambda) \sim j(-1)^{m+1}\mu_1(\lambda^2 - k_o^2)^{1/2} \tag{27}$$

$$\text{when } \left(\frac{n_1 B}{\lambda_o}\right)\sqrt{1 - 1/n_1^2} = (m - 1/2)/2$$

and

$$D_m(\lambda) \sim (-1)^{m+1}n_1^2(\lambda^2 - k_o^2)^{1/2} \tag{28}$$

$$\text{when } \left(\frac{n_1 B}{\lambda_o}\right)\sqrt{1 - 1/n_1^2} = (m-1)/2 \quad.$$

(We are arbitrarily choosing the branch of u_1 in Eq. (7) and (8) so that $u_1 = +j\sqrt{k_1^2 - k_o^2}$ here.)

This branch point singularity at $\lambda = k_o$ in the λ-plane when a mode turns on corresponds to a simple zero in the steepest descent ζ-plane at $\zeta = \pi/2$, since

$$(\lambda^2 - k_o^2)^{1/2} = jk_o\cos\zeta \quad.$$

This simple zero behavior of $D_e(k_o\sin\zeta)$ and $D_m(k_o\sin\zeta)$ causes the point $\zeta = \pi/2$ to become a removable singularity in the $F(\zeta)$ and $G(\zeta)$ functions with

$$F(\zeta) \sim (-1)^m f(k_o) \left(\frac{1}{\mu_1}\right)\left(\frac{-j\omega\mu_o}{8\pi k_1^2} \frac{(1+j)}{\sqrt{\pi}}\right) \text{ (TE Mode)} \tag{29}$$

$$G(\zeta) \sim (-1)^m \frac{g(k_o)}{D_m(k_o)} \left(\frac{1}{\mu_1}\right)\left(\frac{-j\omega\mu_o}{8\pi k_1^2} \frac{j(1+j)}{\sqrt{\pi}}\right) \text{ (TE Mode)} \tag{30}$$

and

$$G(\zeta) \sim j(-1)^m \frac{g(k_o)}{D_e(k_o)} \left(\frac{1}{\mu_1\epsilon_1}\right)\left(\frac{-j\omega\mu_o}{8\pi k_1^2} \frac{j(1+j)}{\sqrt{\pi}}\right) \text{ (TM Mode)} \tag{31}$$

as $\zeta \to \pi/2$ in each case. Equation (29) implies that Π_x^R remains nonzero, in general, as $\theta \to \pi/2$ when a TE mode turns on. Similarly, Eq. (31) implies that

Π_z^R remains in general nonzero as $\theta \to \pi/2$ when a TM mode turns on. In addition, Eq. (30) appears to imply that Π_z^R can also remain nonzero when a TE mode turns on. However, when a TE mode turns on, $g(k_o) = 0$. These results indicate then that E_ϕ^R can extend down to a nonzero value at the horizon only when a TE mode turns on, while E_θ^R can remain nonzero only when a TM mode turns on. E_ϕ^R and E_θ^R determine the $\overline{H}$-plane ($\phi = \frac{\pi}{2}$) and $\overline{E}$-plane ($\phi = 0$) radiation patterns respectively. Although this result is true in general, the presence of the term $\sinh(u_1 z_o)$ in $f(\lambda)$ and $g(\lambda)$ causes exceptional cases to occur. In particular, the $\overline{E}$- and $\overline{H}$-plane radiation patterns will have a null at the horizon even when a surface wave mode is at cutoff for the exceptional case of z_o satisfying the relation

$$\sin\left[k_o z_o \sqrt{n_1^2 - 1} \; \right] = 0 \tag{32}$$

or

$$\frac{n_1 z_o}{\lambda_o} = \frac{p/2}{\sqrt{1 - 1/n_1^2}} \quad , \quad p = 0,1,2,\ldots \quad . \tag{33}$$

Comparing this result with Eq. (26), it is observed that the exceptional case involving a TM mode turning on ($\overline{E}$-plane radiation into the horizon) implies

$$\frac{n_1 (B - z_o)}{\lambda_o} = \frac{\ell/2}{\sqrt{1 - 1/n_1^2}} \quad , \quad \ell = 0,1,2,\ldots \quad . \tag{34}$$

For most practical situations $\ell = 0$, so $z_o = B$; i.e., the antenna is printed on the interface of the substrate and free space. Similarly, if Eq. (33) is compared with Eq. (25), then the exceptional case for a null in the $\overline{H}$-plane pattern at $\theta = \pi/2$ with a TE mode turning on occurs when

$$\frac{n_1 (B - z_o)}{\lambda_o} = \frac{(\ell + \frac{1}{2})/2}{\sqrt{1 - 1/n_1^2}} \quad , \quad \ell = 0,1,\ldots \quad . \tag{35}$$

This criterion cannot be satisfied for the TE_1 mode ($m = 1$) for $z_o > 0$, and therefore there will be nonzero $\overline{H}$-plane radiation into the horizon when the TE_1 mode turns on regardless of the dipole position z_o. A null at $\theta = \pi/2$ can

appear, however, for higher order TE modes.

These results extend directly to the case of Figure 1b. $\bar{H}$-plane radiation into the horizon occurs for a TE mode turning on [15], giving the condition

$$\frac{n_2 t}{\lambda_o} = \frac{n_2}{2\pi\sqrt{n_2^2 - 1}} \tan^{-1}\left[\frac{\mu_2}{\mu_1} \frac{\sqrt{n_1^2 - 1}}{\sqrt{n_2^2 - 1}} \cot\left(2\pi \frac{n_1 B}{\lambda_o} \sqrt{1 - 1/n_1^2}\right)\right] \qquad (36)$$

while $\bar{E}$-plane radiation into the horizon occurs for a TM mode turning on, or when the condition

$$\frac{n_2 t}{\lambda_o} = \frac{n_2}{2\pi\sqrt{n_2^2 - 1}} \tan^{-1}\left[-\frac{\varepsilon_2}{\varepsilon_1} \frac{\sqrt{n_1^2 - 1}}{\sqrt{n_2^2 - 1}} \tan\left(2\pi \frac{n_1 B}{\lambda_o} \sqrt{1 - 1/n_1^2}\right)\right] \qquad (37)$$

is satisfied.

In a similar manner, as with the single layer, there is the exceptional case where radiation vanishes at $\theta = \pi/2$ despite the surface wave mode turn on condition. This case is still given by Eq. (33) with n_1 corresponding to the lower layer material (the dipole is assumed to be within the lower layer here). This does not constrain the dipole from being at the substrate-superstrate interface ($z_o = B$) in achieving radiation into the horizon in either the $\bar{E}$-plane or the $\bar{H}$-plane, since B is now arbitrary. In fact, $\frac{n_1 B}{\lambda_o} \sqrt{1 - 1/n_1^2} \neq p/2$, unless the top layer is of thickness

$$\frac{n_2 t}{\lambda_o} \sqrt{1 - 1/n_2^2} = (\ell + 1/2)/2 \quad , \quad \ell = 0, 1, \ldots \quad \text{(TE Mode)}$$

or

$$\frac{n_2 t}{\lambda_o} \sqrt{1 - 1/n_2^2} = \frac{\ell}{2} \quad , \qquad \ell = 0, 1, \ldots \quad \text{(TM Mode)} .$$

For this reason, $\bar{E}$- and $\bar{H}$-plane radiation into the horizon is always observed in practical cases involving a dipole at the substrate-superstrate interface in the geometry of Figure 1b.

III. A RAY OPTICS INTERPRETATION

A ray picture can be composed in order to provide an explanation of the radiation into the horizon effect. With reference to Figure 3, we have plane

wave spectrum rays emanating from the dipole and reflecting between the ground plane and the dielectric interface, with the rays partially transmitting into space at each reflection from the interface. For far-field radiation at an angle θ, the reflection angle within the dielectric is θ_1, determined from Snell's law $n_1\sin\theta_1 = \sin\theta$. There are two such rays which leave the dipole as shown in the figure. The reflection coefficient for the rays at $z = B$ is

$$\Gamma = \frac{Z_a - Z_d}{Z_a + Z_d} \tag{38}$$

where

$$Z_a = \dot{n}_0\cos\theta \tag{39}$$

$$Z_d = \eta_0\sqrt{\frac{\mu_1}{\epsilon_1}}\ \cos\theta_1 \tag{40}$$

for $\overline{E}$ in the plane of incidence ($E_{||}$), and

$$Z_a = \eta_0\sec\theta \tag{41}$$

$$Z_d = \eta_0\sqrt{\frac{\mu_1}{\epsilon_1}}\ \sec\theta_1 \tag{42}$$

for $\overline{E}$ normal to the plane of incidence ($E_\perp$), where $\eta_0 = \sqrt{\frac{\mu_0}{\epsilon_0}}$. The E_θ component of the radiated field corresponds to $E_{||}$ while the E_ϕ component corresponds to $E_\perp$. In either case, $|\Gamma| \to 1$ as $\theta \to \pi/2$. Rays are increasingly trapped in the substrate as $\theta \to \pi/2$ and radiation into space goes to zero with the only excepti possible when the rays add up in phase after each bounce as $\theta \to \pi/2$. This condition arises when a TE mode turns on for $E_\perp$ and when a TM mode turns on for $E_{||}$. A proof can be provided by considering that as the ray travels from a to b its radiation contribution experiences a phase shift ϕ_{ab} given by

$$\phi_{ab} = \pm\pi + \arg(\Gamma) + \Delta_{ab} + k_0 d_{ab}\ . \tag{43}$$

The term $\pm\pi$ in Eq. (43) results from the phase reversal of the tangential $\overline{E}$-field at $z = 0$ (This is the component for which reflection is being considered. A similar analysis applies to the normal component). Similarly, $\arg(\Gamma)$ comes from the phase shift introduced by reflection at the interface (point a). As $\theta \rightarrow \pi/2$ $\arg(\Gamma) = \pm\pi$ for $E_{||}$ and $\arg(\Gamma) = 0$ for $E_{\perp}$. The term Δ_{ab} represents the phase shift the ray undergoes in travelling from a to b, while $k_o d_{ab}$ is the phase shift due to the array factor effect from the separation at a and b, as seen from an observation point at $\theta = \pi/2$. These phase shift terms can be evaluated using

$$d_{ab} = 2B\tan\theta_1 = \frac{2B}{\sqrt{n_1^2-1}} \tag{44}$$

and

$$\Delta_{ab} = -\beta_x d_{ab} - \beta_z (2B) \tag{45}$$

with

$$\beta_x = k_o n_1 \sin\theta_1 = k_o \tag{46}$$

$$\beta_z = k_o n_1 \cos\theta_1 = k_o \sqrt{n_1^2-1} \quad . \tag{47}$$

Thus ϕ_{ab} is obtained to be

$$\phi_{ab} = \pm\pi + \begin{Bmatrix} 0 & E_{\perp} \\ \pm\pi & E_{||} \end{Bmatrix} - 2k_o B\sqrt{n_1^2-1} \quad . \tag{48}$$

For the ray to add in phase after each bounce, it is required that

$$\phi_{ab} = -2\pi m , \qquad m = 0, \pm 1, \pm 2, \ldots$$

and therefore the following criteria are obtained:

$$\left(\frac{n_1 B}{\lambda_o}\right) = \frac{(m - \frac{1}{2})/2}{\sqrt{1 - 1/n_1^2}} \quad , \qquad m = 1, 2, \ldots \qquad (E_\phi - \text{field}) \tag{49}$$

and

$$\left(\frac{n_1 B}{\lambda_o}\right) = \frac{(m-1)/2}{\sqrt{1-1/n_1^2}} \quad , \qquad m = 1,2,\ldots \qquad (E_\theta - \text{field}) \quad . \qquad (50)$$

These are simply recognized as the conditions for the turning on of the TE and TM modes in the substrate, respectively. Hence, ray optics predicts that E_ϕ and E_θ can remain nonzero as $\theta \to \pi/2$ only when the TE and TM modes turn on, respectively. This agrees with the steepest descent analysis. Ray theory may also be used to provide a simple explanation for those exceptional cases where a null appears at $\theta = \pi/2$, in spite of the fact that a mode is at cutoff. To see this, the phase difference between the two plane wave spectrum rays that leave the dipole must be considered. This phase difference is given by

where
$$\phi_{1,2} = \text{Arg}(\Gamma) - 2\beta_z(B-z_o) - \beta_x d_{1,2} + k_o d_{1,2} \qquad (51)$$

$$d_{1,2} = 2(B-z_o)/\sqrt{n_1^2-1} \quad . \qquad (52)$$

The first three terms on the right-hand side of Eq. (51) represent the phase difference due to the reflection of Ray #1 from the interface and the extra distance it travels, while the last term is the array factor term for radiation along the horizon due to the separation of the two rays. Using (46) - (47), and setting $\phi_{1,2} = -(2\ell + 1)\pi$, $\ell = 0, \pm1, \pm2, \ldots$ as the condition for the radiation from the two rays to cancel, there results

$$-(2\ell + 1)\pi = \begin{Bmatrix} 0 & E_\perp \\ \pm\pi & E_{||} \end{Bmatrix} - 2k_o\sqrt{n_1^2 - 1}\,(B - z_o) \quad . \qquad (53)$$

Therefore, the exceptional case for the $\overline{E}$-plane requires that (using $E_{||}$)

$$\frac{n_1(B - z_o)}{\lambda_o} = \frac{\ell/2}{\sqrt{1-1/n_1^2}} \quad , \qquad \ell = 0,1,2,\ldots \qquad (54)$$

while for the $\overline{H}$-plane (using $E_\perp$)

$$\frac{n_1(B - z_o)}{\lambda_o} = \frac{(\ell + \frac{1}{2})/2}{\sqrt{1-1/n_1^2}} \quad , \qquad \ell = 0,1,2,\ldots \qquad (55)$$

-11-

must hold.

These equations are identical to those derived previously for the exceptional cases, i.e., Eqs. (34) and (35).

IV. ANTENNA LOCATION OPTIMIZATION FOR OMNIDIRECTIONALITY

When radiation into the horizon occurs, the corresponding $\overline{E}$- or $\overline{H}$-plane pattern broadens and remains nonzero as $\theta \to \pi/2$. In some cases, this may cause the pattern to become very nearly omnidirectional, depending on the dipole height z_o. Figure 4 shows $\overline{E}$-plane radiation patterns with the TM_2 mode (m = 2) turning on for various dipole positions in the geometry of Figure 1a. The patterns remain nonzero at $\theta = \pi/2$ in all except the last one where $z_o = B$, which is the exceptional case. Of particular interest is the case where $\frac{n_1 z_o}{\lambda_o} = 0.375$. This pattern is omnidirectional to within the width of the grid lines. Similarly, Figure 5 shows $\overline{H}$-plane patterns for different values of z_o with the TE_1 mode (m = 1) turning on, with $\frac{n_1 z_o}{\lambda_o} = 0.188$ corresponding to almost perfect omnidirectionality. In fact, the deviation of this pattern from omnidirectionality is only ≈ 0.002 dB, which cannot be distinguished on the plot. Plots of the $\overline{E}$- and $\overline{H}$-plane patterns for the case of Figure 1b would be similar in appearance to these, showing nearly omnidirectional behavior for certain choices of z_o. An effective criterion can be developed for choosing the dipole height z_o to achieve very nearly omnidirectional patterns. The criterion is to choose z_o so that the radiation power density is equal at $\theta = 0$ and $\theta = \pi/2$. For each case of $\overline{E}$- and $\overline{H}$-plane radiation, this gives a transcendental equation for the normalized dipole height $\frac{n_1 z_o}{\lambda_o}$ which must be solved. The numerical solution is shown in Figures 6a and 6b for the case of a nonmagnetic substrate ($\mu_1 = 1.0$) for the TM_2 and TE_1 modes at cutoff respectively. Figures 7a and 7b show the solution for $\frac{n_1 B}{\lambda_o}$ for the geometry of Figure 1b when $z_o = B$ for nonmagnetic layers, with curves shown for various substrate dielectric constants ϵ_1 (for the TM_2 and TE_1 modes, respectively).

As an illustration of how well this method works, Figure 8 shows $\overline{E}$-plane patterns corresponding to several different ϵ_1 values of Figure 6a. As ϵ_1 tends to 1.0, the degree of omnidirectionality obtained using this criterion worsens. For $\epsilon_1 \geq \sim 2.0$, the patterns are omnidirectional to within the width of the lines and cannot be distinguished on the plots, so only cases with $\epsilon_1 \leq 2.0$ are shown.

Although it is easy to obtain nearly omnidirectional patterns this way, this may not be the desired goal for certain applications. In some cases, it may be desired to suppress the radiation in a certain direction by a specified amount relative to the peak field strength. This can be achieved by slightly modifying the appropriate transcendental equation for the dipole position. Figures 9a and 9b show cases for which a desired 10 dB suppression at $\theta = 0$ has been achieved for the cases of $\overline{E}$- and $\overline{H}$-plane radiation into the horizon.

V. CONCLUSION

It has been seen that the radiation patterns for printed antennas always tend to zero as $\theta \to \pi/2$ unless a surface wave mode is exactly at cutoff. When a TE mode turns on, the $\overline{H}$-plane pattern remains nonzero at $\theta = \pi/2$, and when a TM mode turns on the $\overline{E}$-plane pattern remains nonzero at $\theta = \pi/2$. The only exceptions are for $\dfrac{n_1 z_0}{\lambda_0} \sqrt{1-1/n_1^2} = p/2$, $p = 0,1,2,\ldots$.

These results can be explained from the coinciding of a pole and a branch point in the complex plane for the Sommerfeld integrals, which causes a removable singularity to occur in the steepest descent integrations for the far field. A ray optics interpretation has been given to help explain the phenomenon physically. In addition, a criterion for choosing the antenna position within a substrate to achieve a nearly omnidirectional $\overline{E}$- or $\overline{H}$-plane pattern has been given and graphs showing this optimum antenna location are presented. These results are extended to the case of an antenna at the interface of a substrate-superstrate geometry involving different materials. Plots are shown

-13-

to indicate the degree of omnidirectionality obtainable with this method and its limitations for small ϵ. Finally, it is indicated that the criterion can be extended to produce $\overline{E}$- or $\overline{H}$-plane patterns with arbitrary suppression at a desired angle θ.

REFERENCES

[1] N. K. Uzunoglu, N. G. Alexopoulos, and J. G. Fikioris, "Radiation Properties of Microstrip Dipoles," IEEE Trans. Antennas Propagat., Vol. AP-27, pp. 853-858, Nov. 1979. (See also Correction, IEEE Trans. Antennas Propagat., Vol. AP-30, p. 526, May 1982.)

[2] I. E. Rana and N. G. Alexopoulos, "Current Distribution and Input Impedance of Printed Dipoles," IEEE Trans. Antennas Propagat., Vol. AP-29, pp. 99-105, Jan. 1981. Note that Equations (13) and (14) have a factor of 2, which is a misprint.

[3] N. G. Alexopoulos and I. E. Rana, "Mutual Impedance Computation Between Printed Dipoles," IEEE Trans. Antennas Propagat., Vol. AP-29, pp. 106-111, Jan. 1981.

[4] N. G. Alexopoulos and I. E. Rana, "Current Distribution and Input Impedance of Printed Dipoles," Correction, IEEE Trans. Antennas Propagat., Vol. AP-30, p. 822, July 1982.

[5] P. B. Katehi and N. G. Alexopoulos, "On the Effect of Substrate Thickness and Permittivity on Printed Circuit Dipole Properties," IEEE Trans. antennas Propagat., Vol. AP-30, pp. 34-39, January 1983. Note that far-field Π_θ and Π_ϕ are defined here with a factor of 1/2, so that $E_\theta \sim 2k_o^2\Pi_\theta$ and $E_\phi \sim 2k_o^2\Pi_\phi$.

[6] P. B. Katehi and N. G. Alexopoulos, "Real Axis Integration of Sommerfeld Integrals with Applications to Printed Circuit Antennas," J. Math. Phys. 24(3), pp. 527-533, March 1983.

[7] N. G. Alexopoulos, P. B. Katehi, and D. B. Rutledge, "Substrate Optimization for Integrated Circuit Antennas," IEEE Trans. Microwave Theory Tech., Vol. MTT-31, pp. 550-557, July 1983.

[8] D. M. Pozar, "Input Impedance and Mutual Coupling of Rectangular Microstrip Antennas," IEEE Trans. Antennas Propagat., Vol. AP-30, pp. 1191-1196, Nov. 1982.

[9] D. M. Pozar, "Considerations for Millimeter Wave Printed Antennas," IEEE Trans. Antennas Propagat., Vol. AP-31, pp. 740-747, Sept. 1983.

[10] A. Sommerfeld, Partial Differential Equations, Academic Press, New York, 1962.

[11] L. M. Brekhovskikh, Waves in Layered Media, Academic Press, New York, 1960.

[12] A. Baños, Jr., Dipole Radiation in the Presence of a Conducting Half-Space, Pergamon Press, New York, 1966.

[13] J. R. Wait, Electromagnetic Waves in Stratified Media, Second Edition, Pergamon Press, New York, 1970.

[14] L. Tsang and J. A. Kong, "Interference Patterns of a Horizontal Electric Dipole over Layered Dielectric Media," J. Geophys. Res., Vol. 78, pp. 3287-3300, June 1973.

[15] N. G. Alexopoulos and D. R. Jackson, "Fundamental Superstrate (Cover) Effects on Printed Circuit Antennas," to appear in IEEE Trans. Antennas Propagat.

FIGURE CAPTIONS

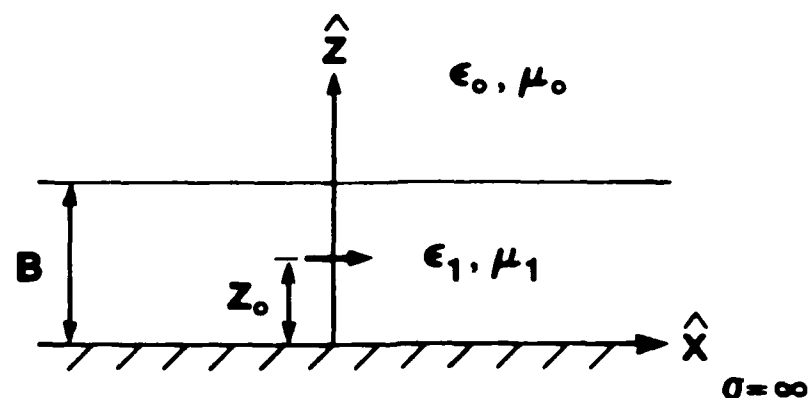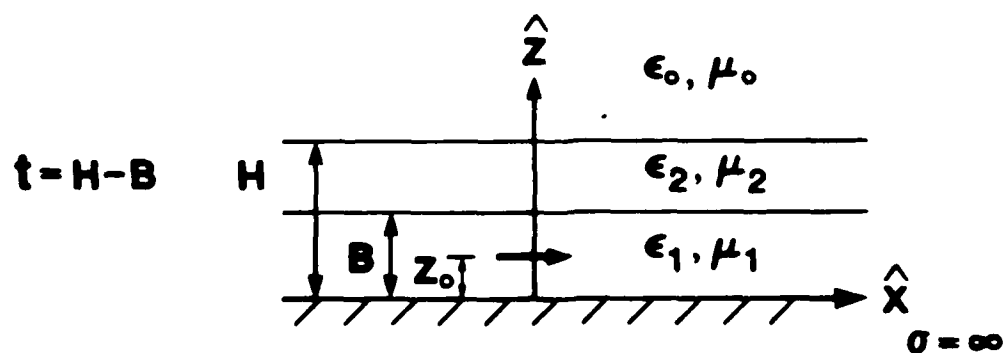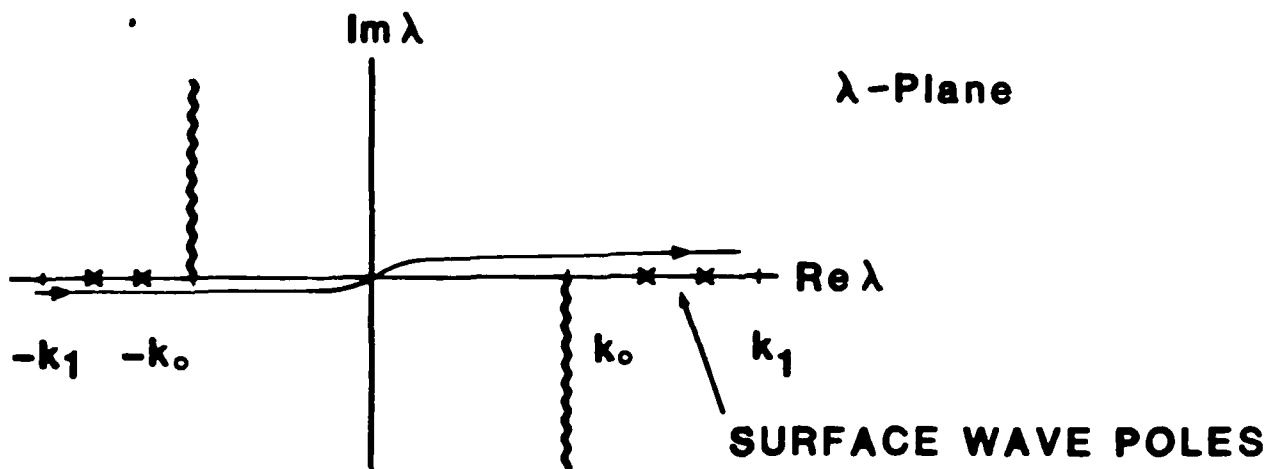|	
Figure 1a	– Substrate with Dipole Embedded
Figure 1b	– Dipole in Substrate with Superstrate
Figure 2a	– Sommerfeld Contour of Integration
Figure 2b	– Steepest Descent Contour of Integration
Figure 2c	– Steepest Descent contour for $\theta = \pi/2$
Figure 3	– Ray Optics Geometry
Figure 4a	– $\overline{E}$-Plane Radiation into the Horizon for Different Values of $\dfrac{n_1 z_o}{\lambda_o}$
Figure 4b	– $\overline{E}$-Plane Radiation into the Horizon for Different Values of $\dfrac{n_1 z_o}{\lambda_o}$
Figure 4c	– $\overline{E}$-Plane Radiation into the Horizon for Different Values of $\dfrac{n_1 z_o}{\lambda_o}$
Figure 4d	– $\overline{E}$-Plane Radiation into the Horizon for Different Values of $\dfrac{n_1 z_o}{\lambda_o}$
Figure 4e	– $\overline{E}$-Plane Radiation into the Horizon for Different Values of $\dfrac{n_1 z_o}{\lambda_o}$
Figure 4f	– $\overline{E}$-Plane Radiation into the Horizon for Different Values of $\dfrac{n_1 z_o}{\lambda_o}$
Figure 5a	– $\overline{H}$-Plane Radiation into the Horizon for Different Values of $\dfrac{n_1 z_o}{\lambda_o}$
Figure 5b	– $\overline{H}$-Plane Radiation into the Horizon for Different Values of $\dfrac{n_1 z_o}{\lambda_o}$
Figure 5c	– $\overline{H}$-Plane Radiation into the Horizon for Different Values of $\dfrac{n_1 z_o}{\lambda_o}$

Figure 5d — $\overline{H}$-Plane Radiation into the Horizon for Different Values of $\dfrac{n_1 z_o}{\lambda_o}$

Figure 6a — $\dfrac{n_1 z_o}{\lambda_o}$ vs. ε_1 for $\overline{E}$-Plane Omni-directionality Condition

Figure 6b — $\dfrac{n_1 z_o}{\lambda_o}$ vs. ε_1 for $\overline{H}$-Plane Omni-directionality Condition

Figure 7a — $\dfrac{n_1 B}{\lambda_o}$ vs. ε_2 for $\overline{E}$-Plane Omni-directionality Condition

Figure 7b — $\dfrac{n_1 B}{\lambda_o}$ vs. ε_2 for $\overline{H}$-Plane Omni-directionality condition

Figure 8a — $\overline{E}$-Plane Radiation into the Horizon using optimum $\dfrac{n_1 z_o}{\lambda_o}$ condition for different values of ε_1

Figure 8b — $\overline{E}$-Plane Radiation into the Horizon using optimum $\dfrac{n_1 z_o}{\lambda_o}$ condition for different values of ε_1

Figure 8c — $\overline{E}$-Plane Radiation into the Horizon using optimum $\dfrac{n_1 z_o}{\lambda_o}$ condition for different values of ε_1

Figure 8d — $\overline{E}$-Plane Radiation into the Horizon using optimum $\dfrac{n_1 z_o}{\lambda_o}$ condition for different values of ε_1

Figure 9a — $\overline{E}$-Plane 10 dB Suppressed Pattern at $\theta = 0°$. $\varepsilon_1 = 4.0$, $\mu_1 = 1.0$, $\dfrac{n_1 B}{\lambda_o} = 0.580$, $\dfrac{n_1 z_o}{\lambda_o} = 0.480$. (Peak gain is 6.753 dB at $\theta = \pi/2$.)

Figure 9b $-$ $\overline{\text{H}}$-Plane 10 dB Suppressed Pattern

at $\theta = 0^\circ$. $\epsilon_1 = 4.0$, $\mu_1 = 1.0$,

$\dfrac{n_1 B}{\lambda_o} = 0.865$, $\dfrac{n_1 z_o}{\lambda_o} = 0.450$. (Peak

gain is 7.665 dB at $\theta = \pi/2$.)

Figure 1a

Substrate with Dipole Embedded

$t = H - B$

Figure 1b

Dipole in Substrate with Superstrate

Figure 2a

Sommerfeld Contour of Integration
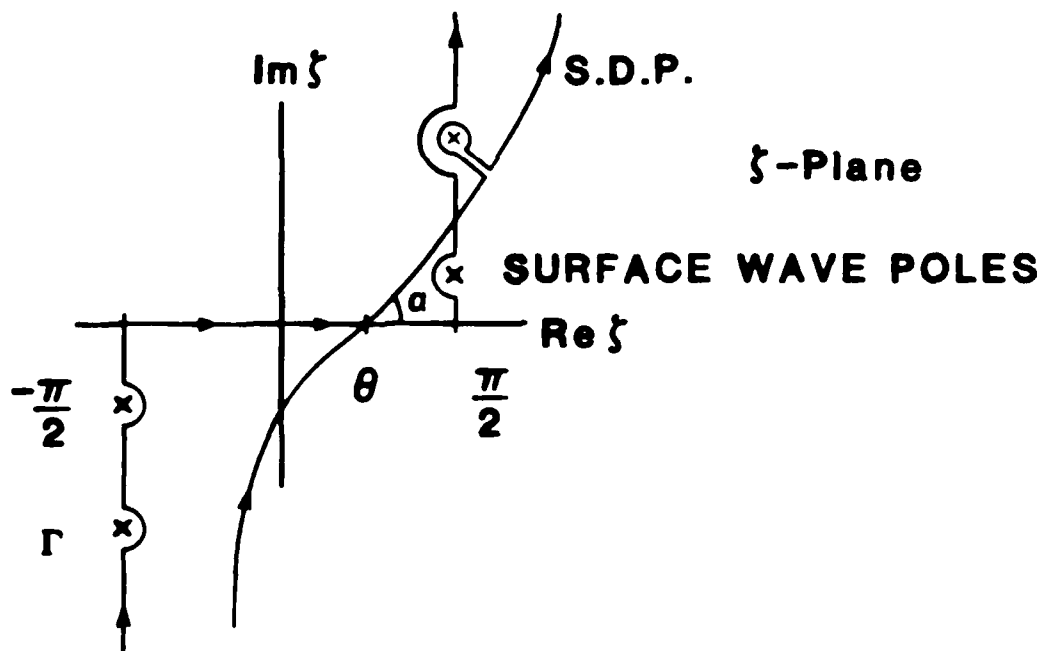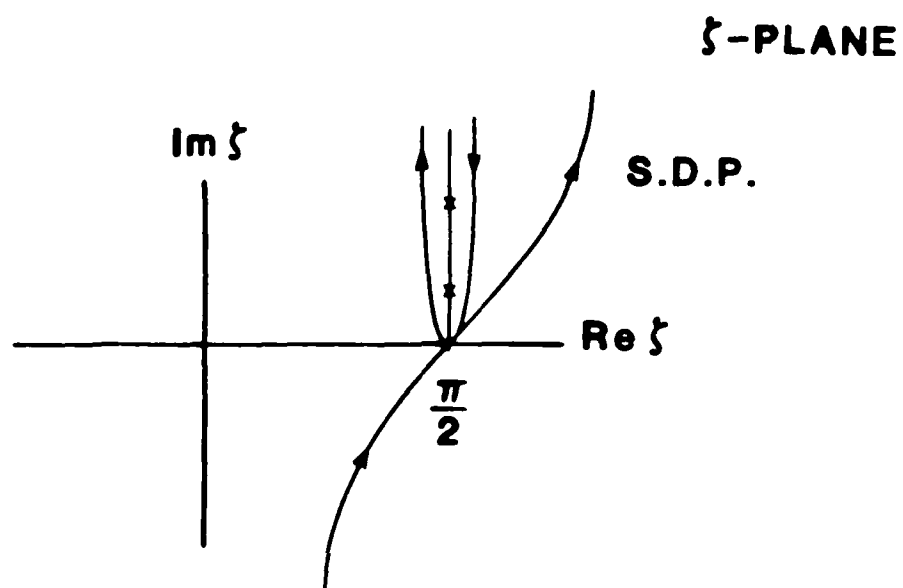

Figure 2b

Steepest Descent Contour of Integration

Figure 2c

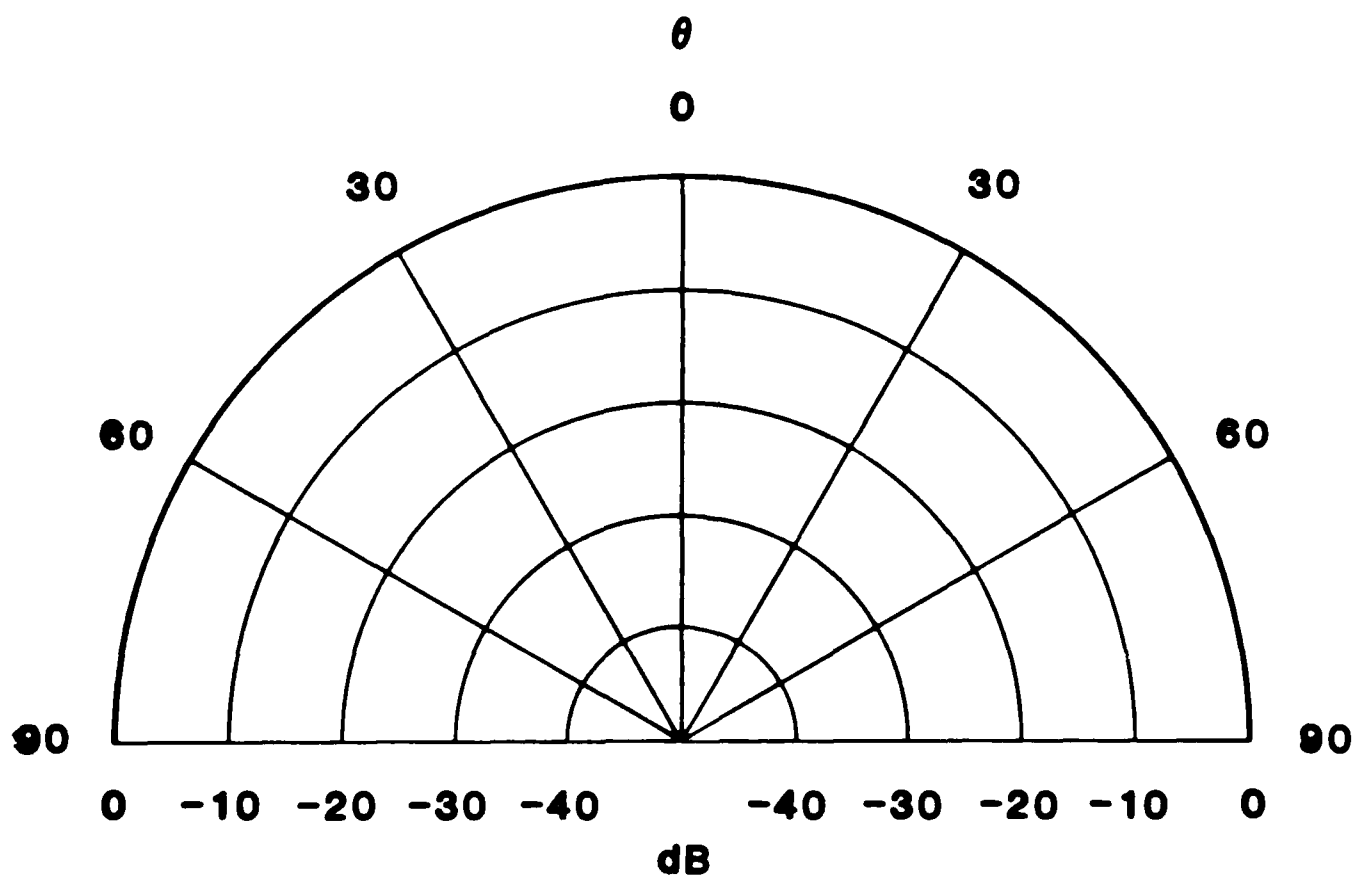**Steepest Descent Contour for** $\theta = \pi/2$
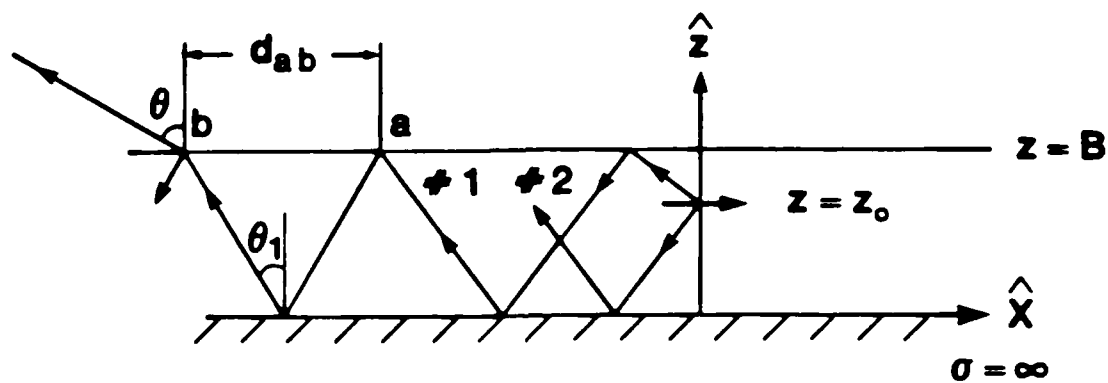
Figure 3

Ray Optics Geometry
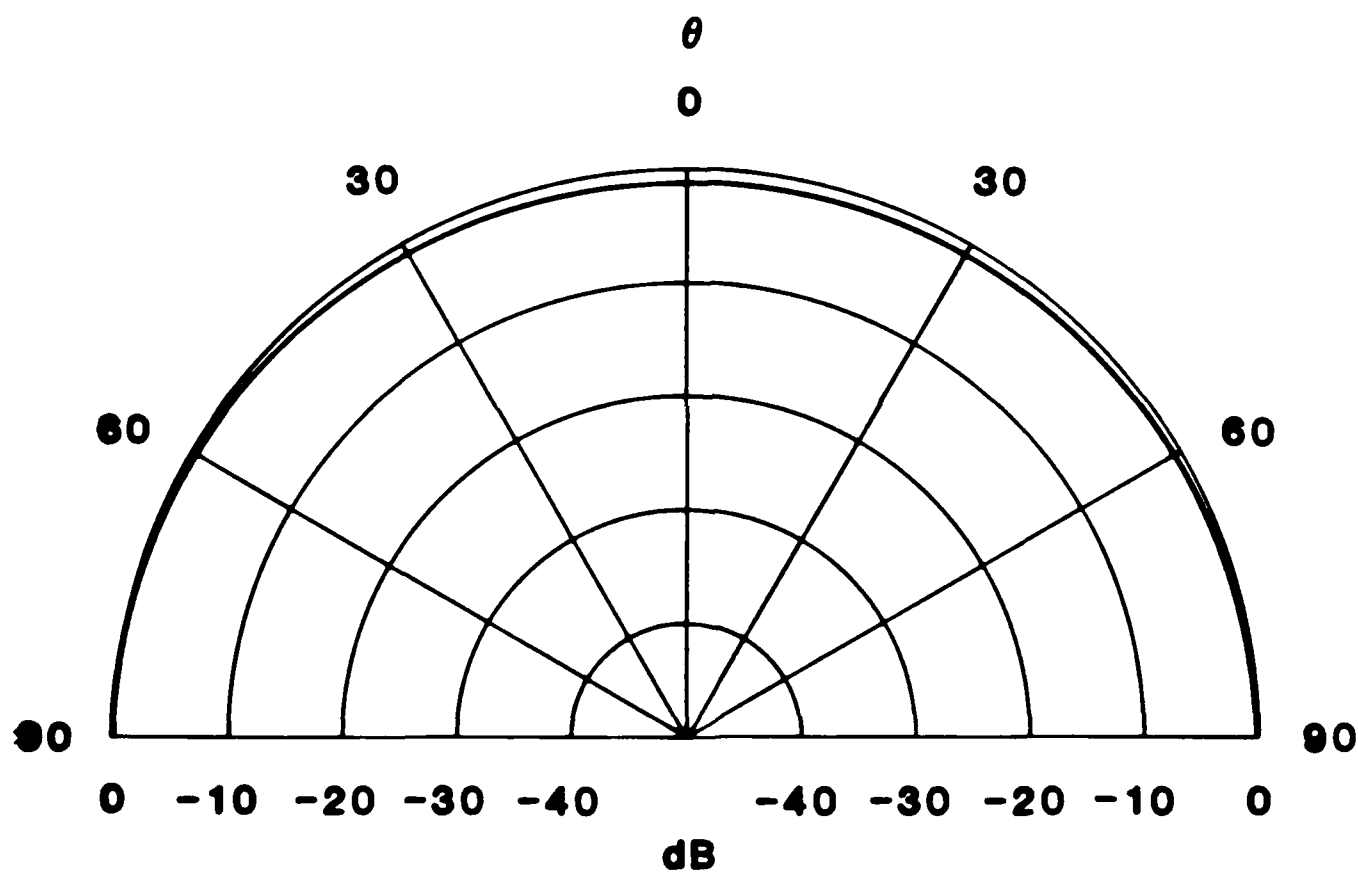
E̅-PLANE PATTERN

$$\epsilon_1 = 4.0 \qquad \frac{n_1 B}{\lambda_o} = .577$$

$$\mu_1 = 1.0 \qquad \frac{n_1 Z_o}{\lambda_o} = .050$$
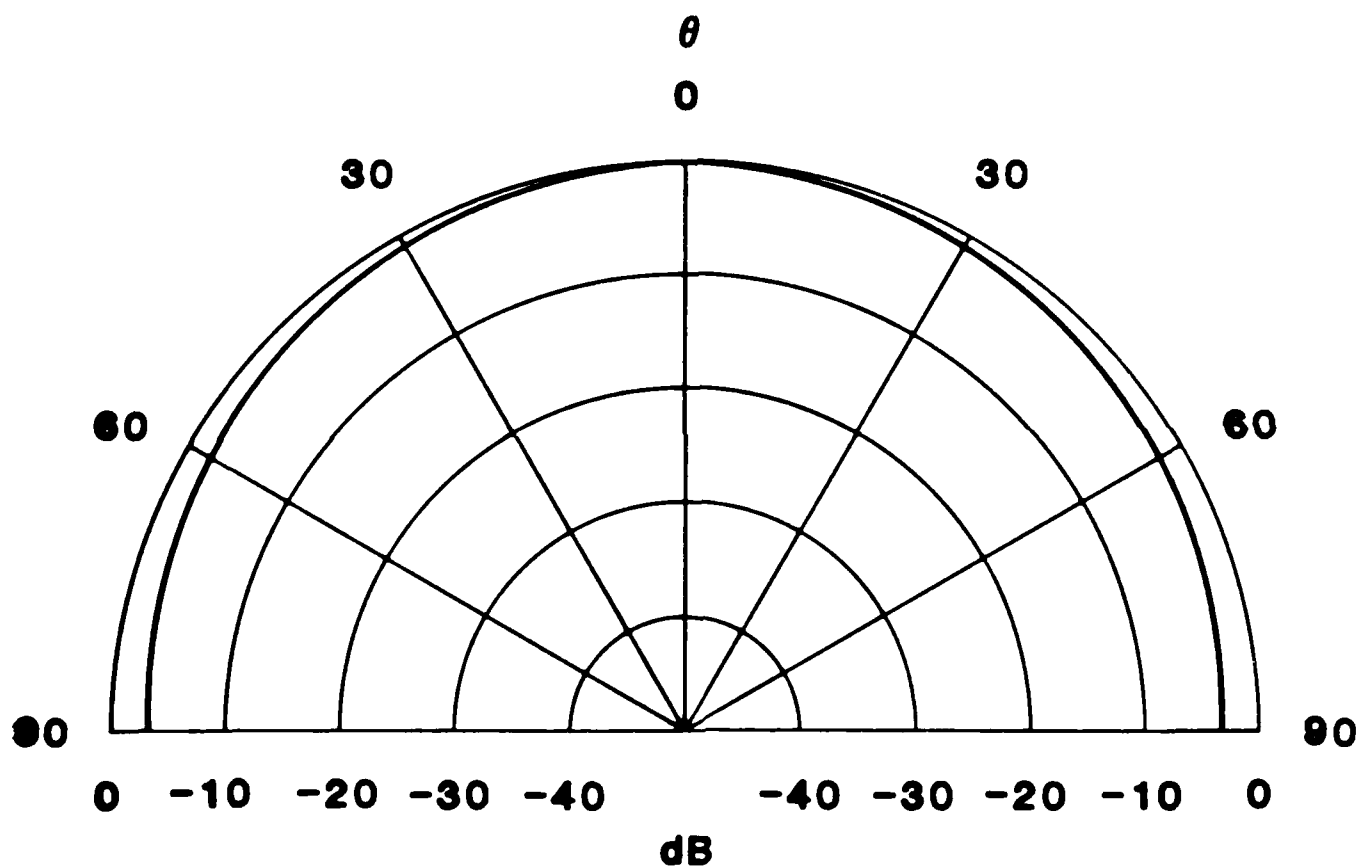
Figure 4a

Ē-PLANE PATTERN

$$\epsilon_1 = 4.0 \qquad \frac{n_1 B}{\lambda_o} = .577$$

$$\mu_1 = 1.0 \qquad \frac{n_1 Z_o}{\lambda_o} = .300$$

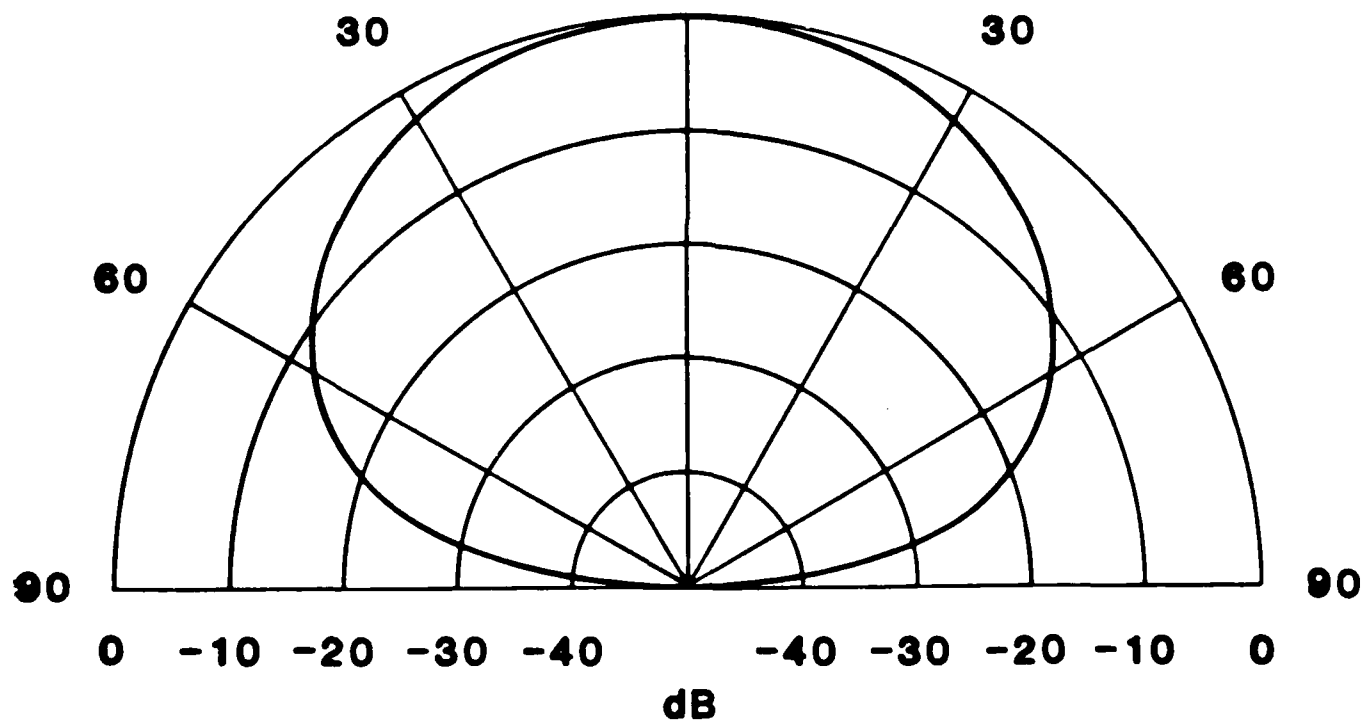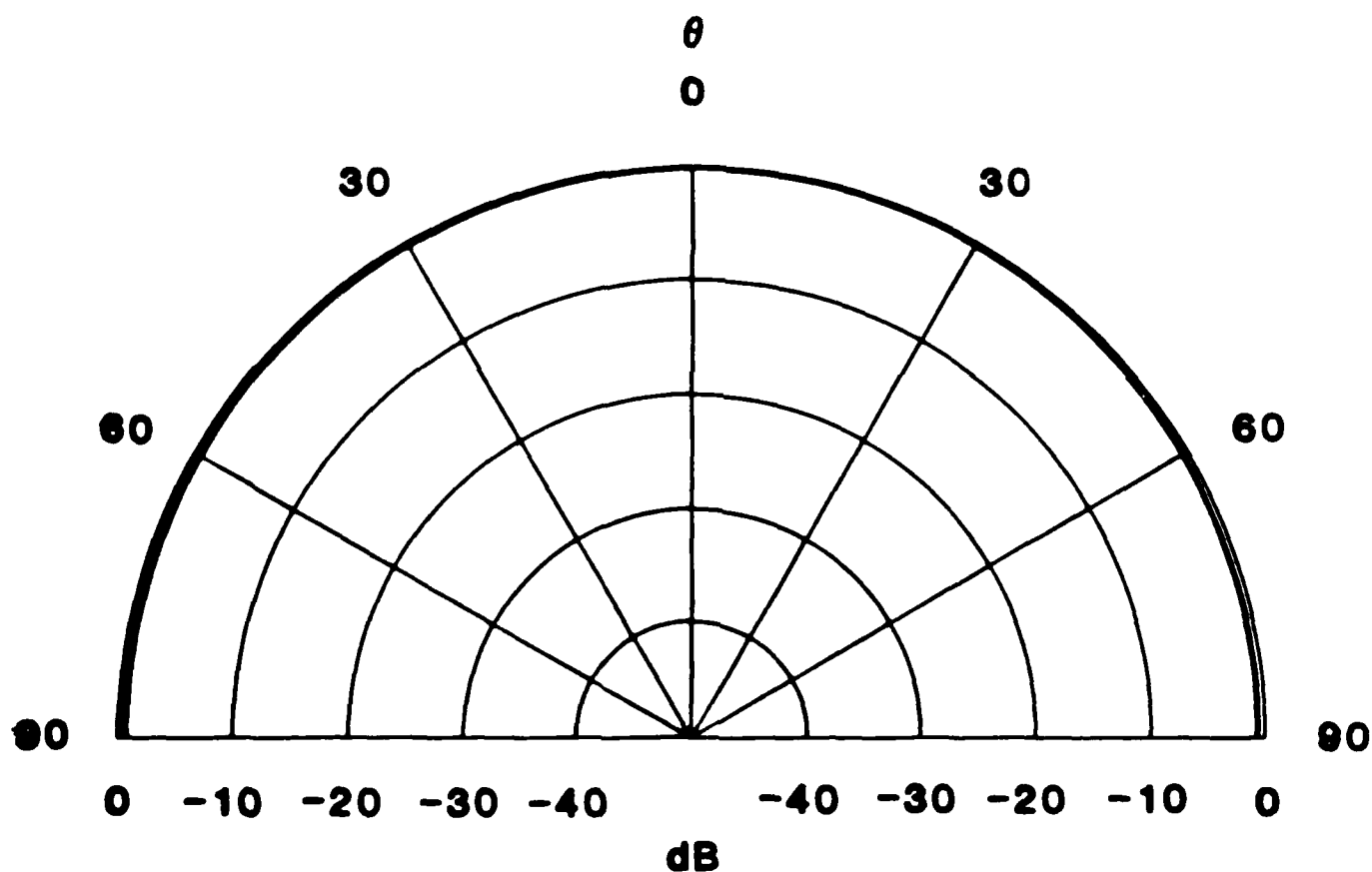θ

0
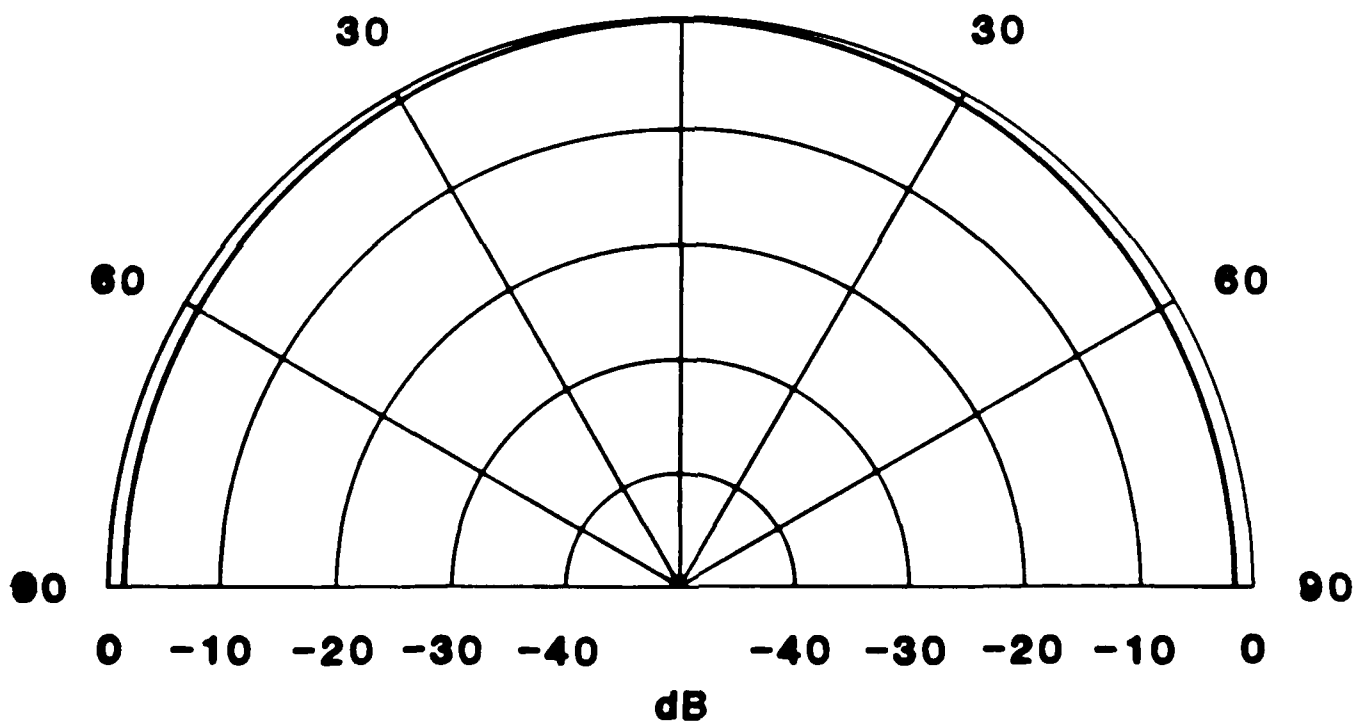
Figure 4b

Ē-PLANE PATTERN

$\epsilon_1 = 4.0$ $\qquad \dfrac{n_1 B}{\lambda_o} = .577$

$\mu_1 = 1.0$ $\qquad \dfrac{n_1 Z_o}{\lambda_o} = .345$
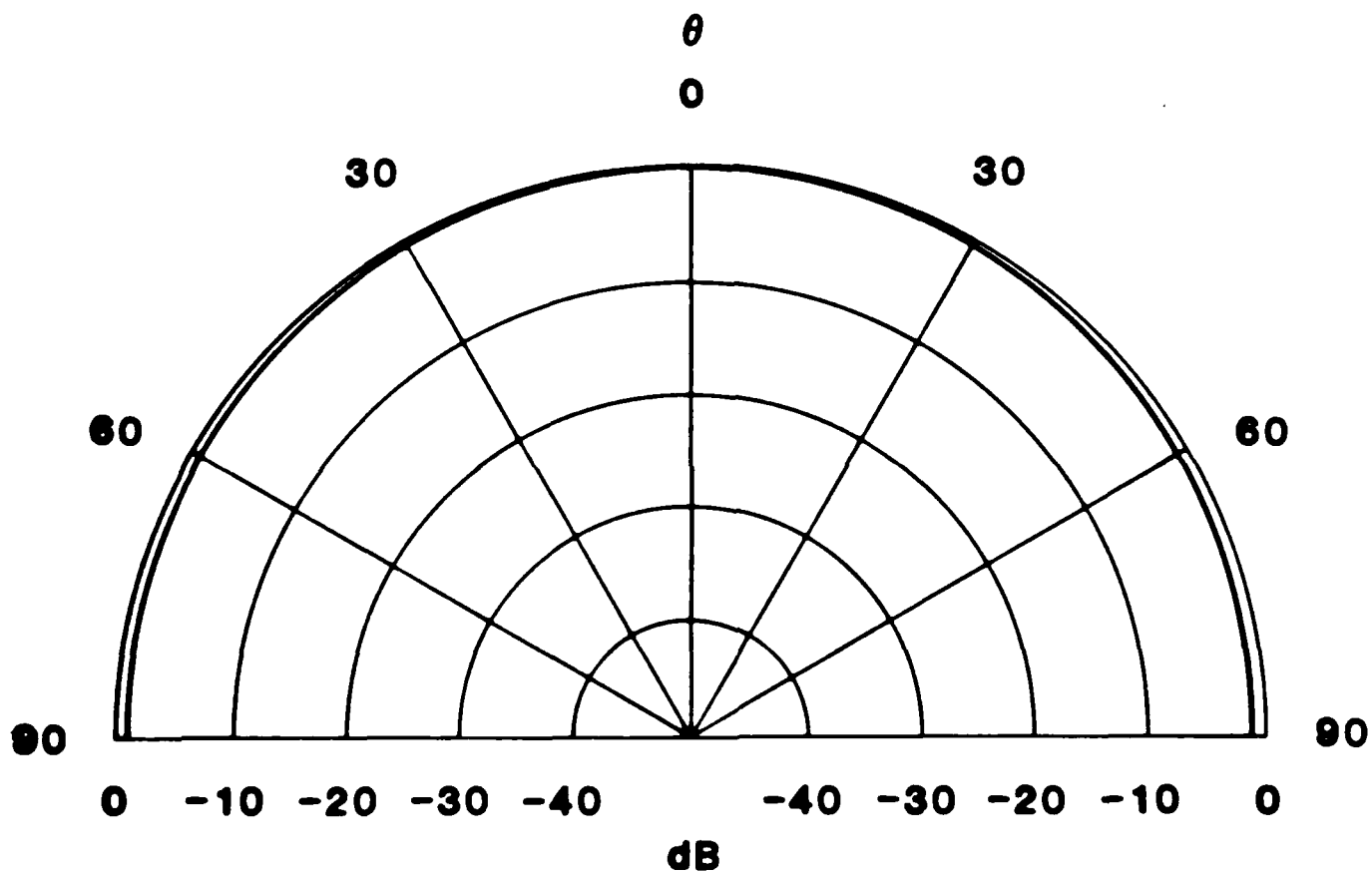
Figure 4c

Ē-PLANE PATTERN

$\epsilon_1 = 4.0$ $\qquad \dfrac{n_1 B}{\lambda_o} = .577$

$\mu_1 = 1.0$ $\qquad \dfrac{n_1 Z_o}{\lambda_o} = .375$

θ

0

30   30

60   60

90   90

0   -10   -20   -30   -40   -40   -30   -20   -10   0

dB

Figure 4d

$\bar{E}$-PLANE PATTERN

$$\epsilon_1 = 4.0 \qquad \frac{n_1 B}{\lambda_o} = .577$$

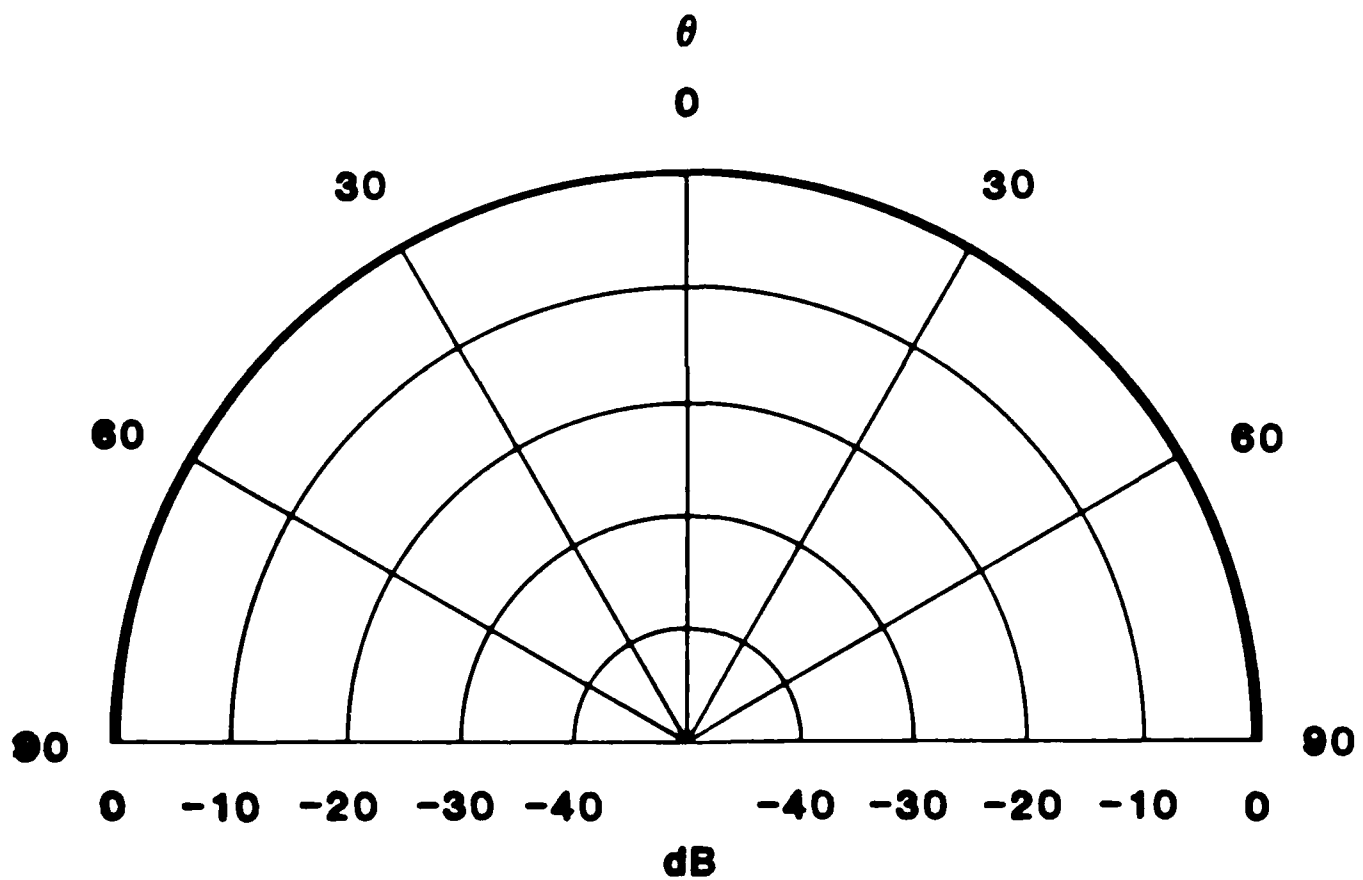$$\mu_1 = 1.0 \qquad \frac{n_1 Z_o}{\lambda_o} = .400$$
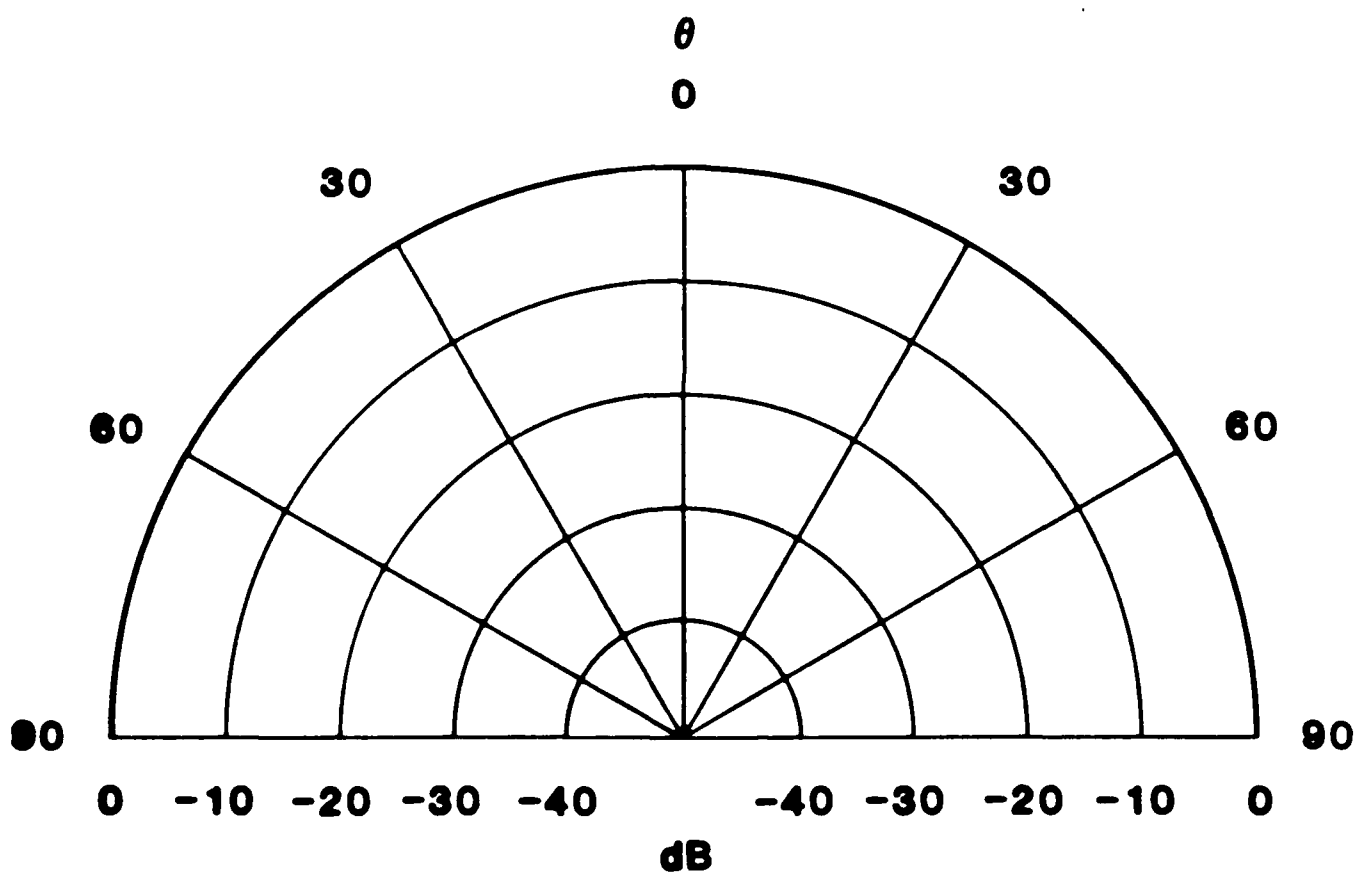

Figure 4e

$\overline{E}$-PLANE PATTERN

$\epsilon_1 = 4.0$ $\qquad \dfrac{n_1 B}{\lambda_o} = .577$

$\mu_1 = 1.0$ $\qquad \dfrac{n_1 Z_o}{\lambda_o} = .577$

Figure 4f

$\overline{H}$-PLANE PATTERN

$\epsilon_1 = 4.0$ $\qquad \dfrac{n_1 B}{\lambda_o} = .289$

$\mu_1 = 1.0$ $\qquad \dfrac{n_1 Z_o}{\lambda_o} = .050$

θ

0

30   30

60   60

90   90

0 −10 −20 −30 −40   −40 −30 −20 −10 0

dB

Figure 5a

$\overline{\text{H}}$-PLANE PATTERN

$\epsilon_1 = 4.0 \qquad \dfrac{n_1 B}{\lambda_o} = .289$
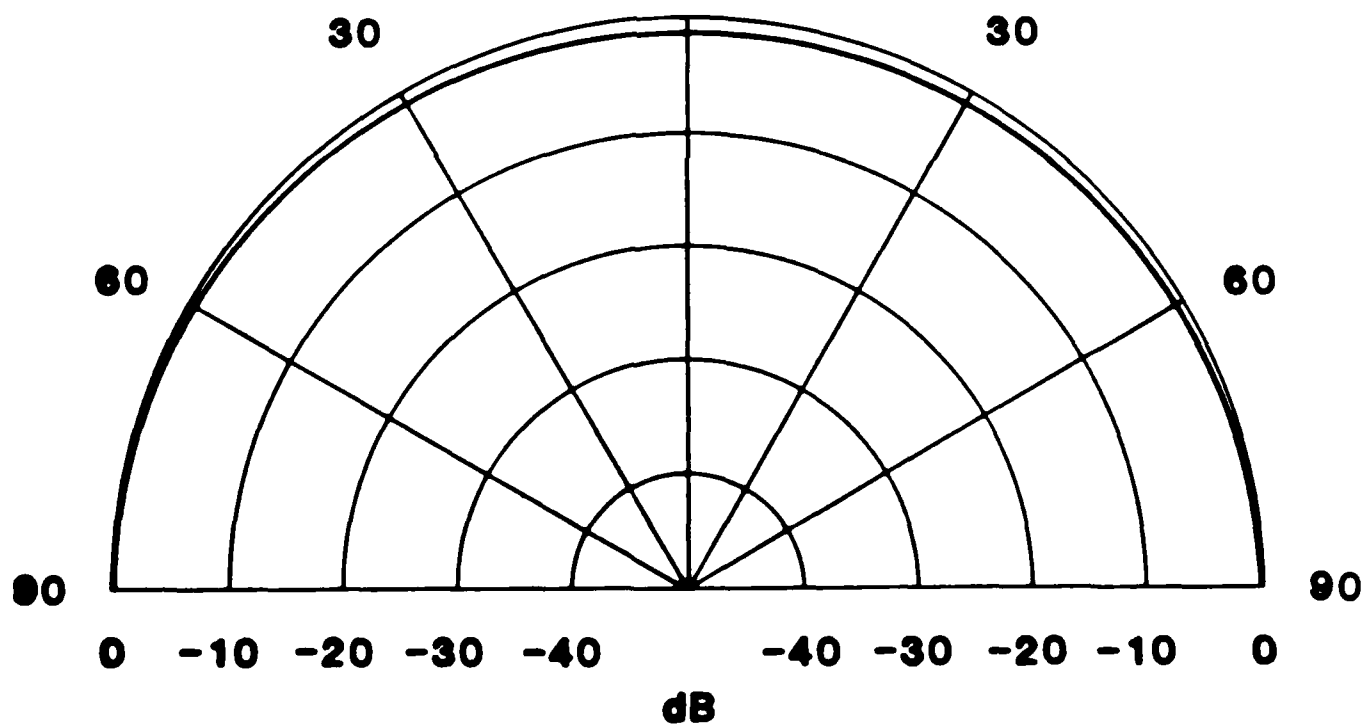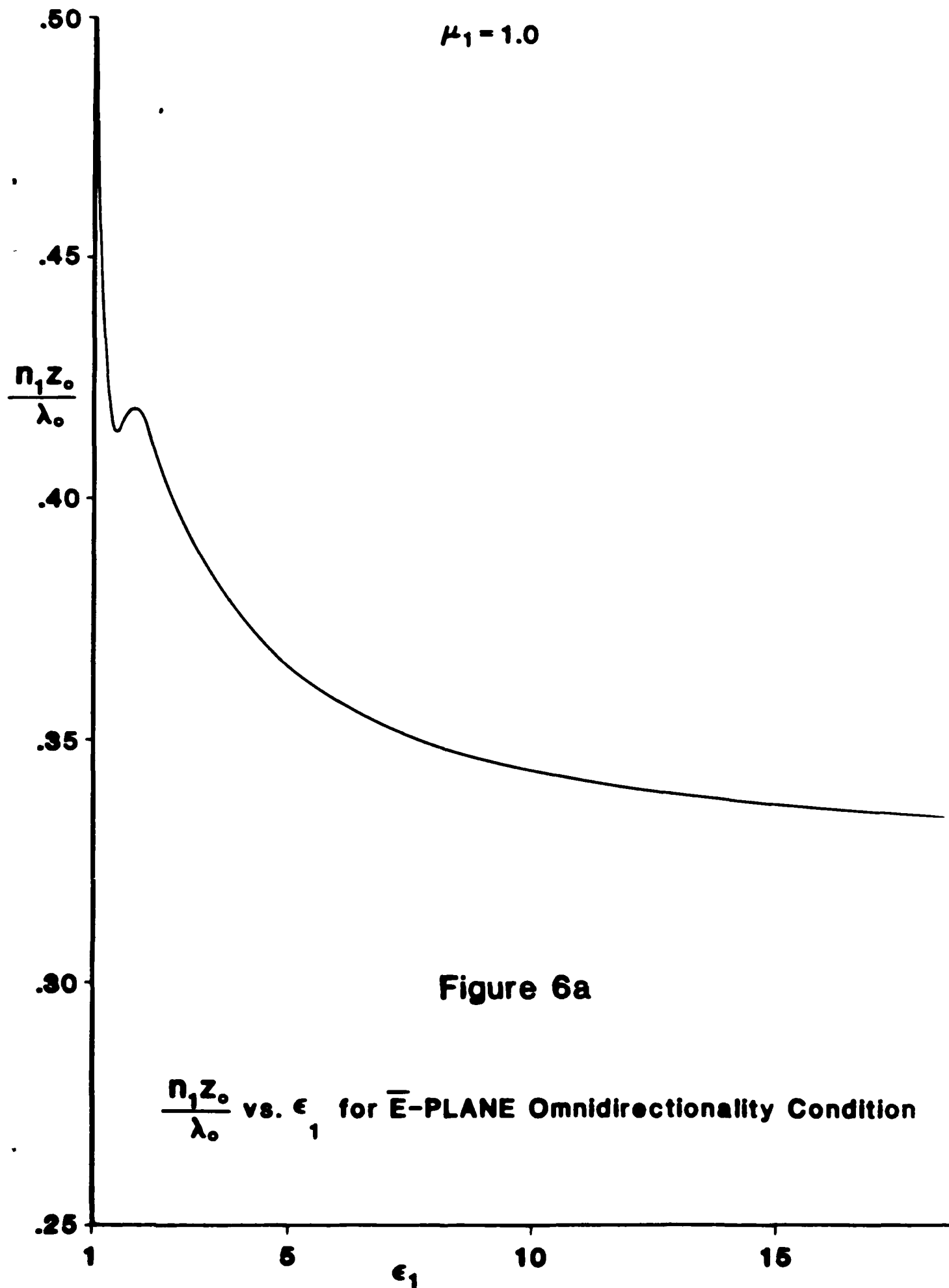
$\mu_1 = 1.0 \qquad \dfrac{n_1 Z_o}{\lambda_o} = .150$

θ

0

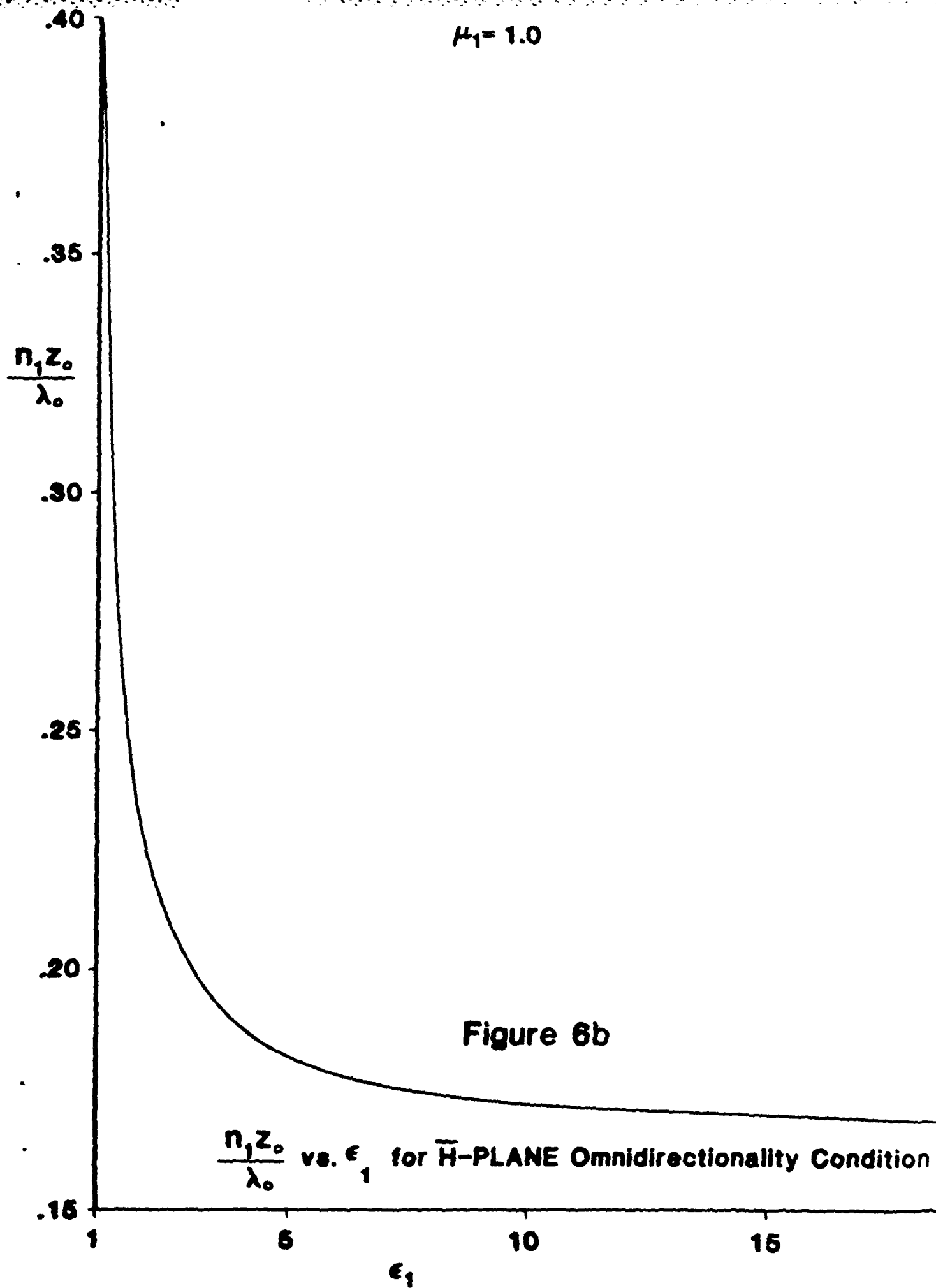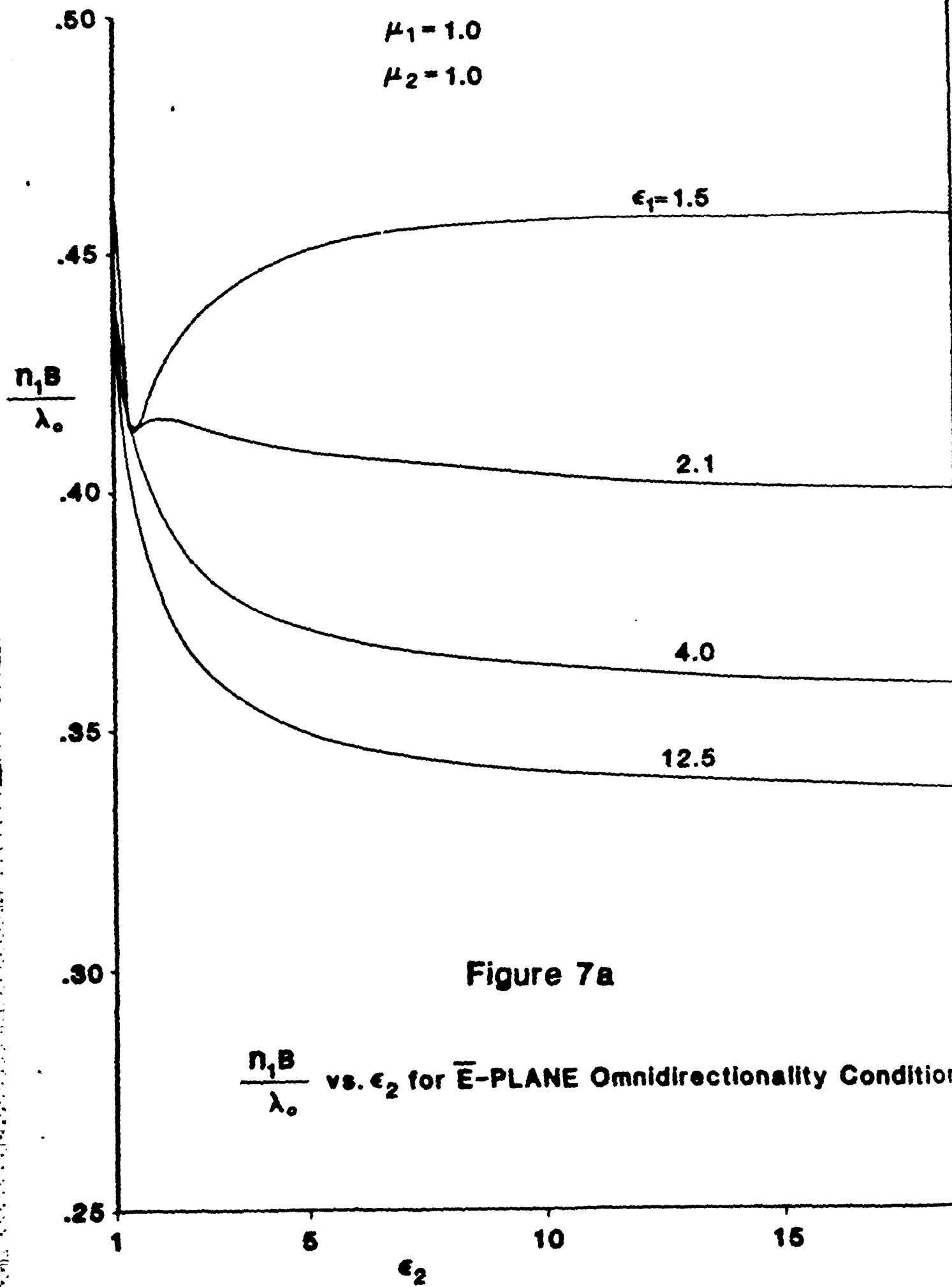30   30

60   60

90   90

0   −10 −20 −30 −40   −40 −30 −20 −10   0

dB

Figure 5b

$\overline{H}$-PLANE PATTERN

$\epsilon_1 = 4.0$ $\dfrac{n_1 B}{\lambda_o} = .289$

$\mu_1 = 1.0$ $\dfrac{n_1 Z_o}{\lambda_o} = .188$

Figure 5c

$\overline{H}$-PLANE PATTERN

$\epsilon_1 = 4.0$ $\dfrac{n_1 B}{\lambda_o} = .289$

$\mu_1 = 1.0$ $\dfrac{n_1 Z_o}{\lambda_o} = .289$

θ

0

Figure 5d

Figure 6a

$\dfrac{n_1 Z_o}{\lambda_o}$ vs. ϵ_1 for $\overline{E}$-PLANE Omnidirectionality Condition

$\mu_1 = 1.0$

$\dfrac{n_1 Z_0}{\lambda_0}$

Figure 6b

$\dfrac{n_1 Z_0}{\lambda_0}$ vs. ϵ_1 for $\overline{H}$-PLANE Omnidirectionality Condition

ϵ_1

Figure 7a

$\frac{n_1 B}{\lambda_o}$ vs. ϵ_2 for $\overline{E}$-PLANE Omnidirectionality Condition

$\mu_1 = 1.0$

$\mu_2 = 1.0$

$\epsilon_1 = 12.5$

4.0

2.1

Figure 7b

1.5

$\dfrac{n_1 B}{\lambda_o}$ vs. ϵ_2 for $\overline{H}$-PLANE Omnidirectionality C(

$\overline{E}$-PLANE PATTERN

$\epsilon_1 = 2.0$ $\dfrac{n_1 B}{\lambda_o} = .707$

$\mu_1 = 1.0$ $\dfrac{n_1 Z_o}{\lambda_o} = .417$
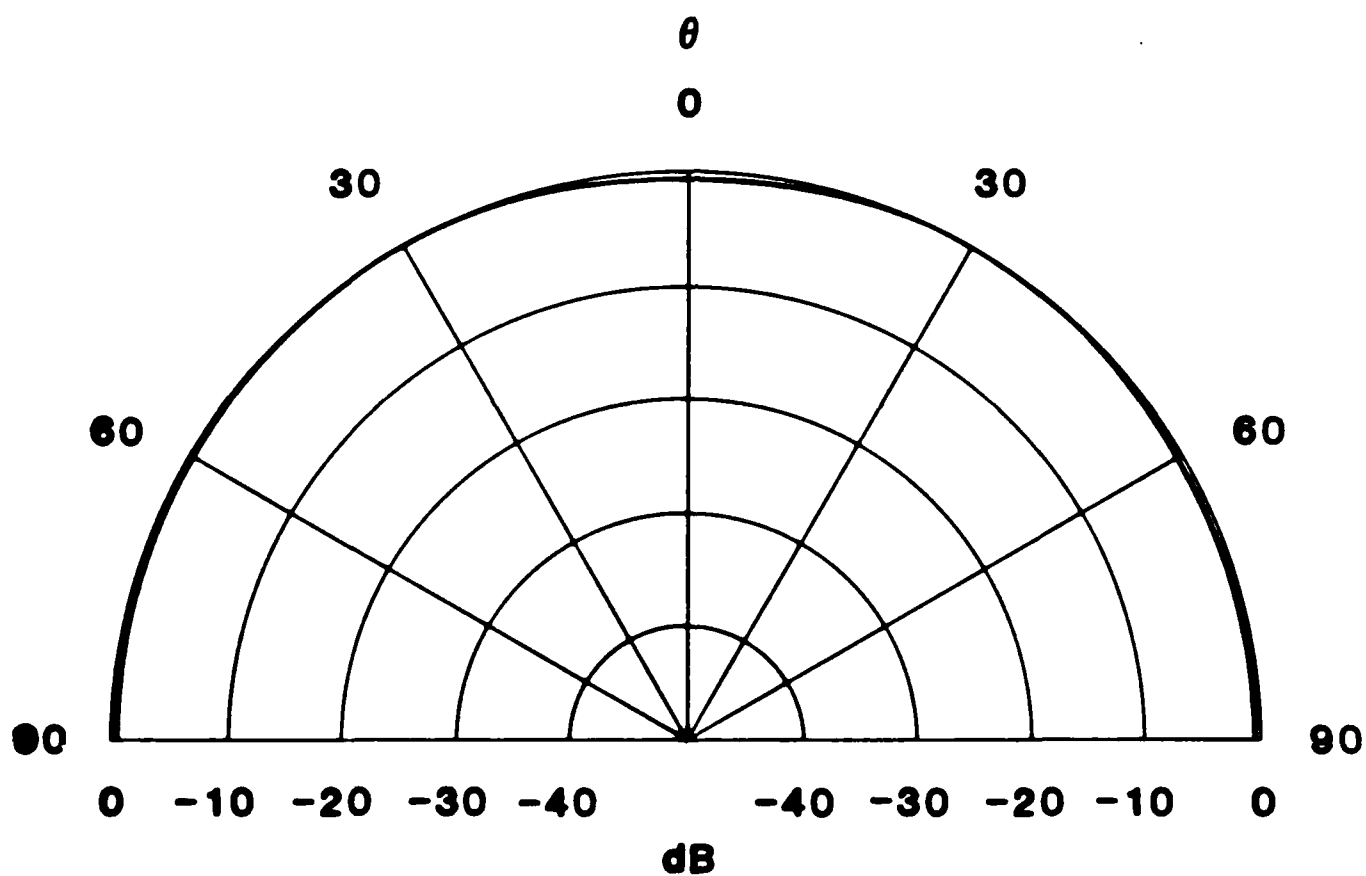
Figure 8a

Ē-PLANE PATTERN

$\epsilon_1 = 1.5$ $\dfrac{n_1 B}{\lambda_o} = .866$

$\mu_1 = 1.0$ $\dfrac{n_1 Z_o}{\lambda_o} = .413$
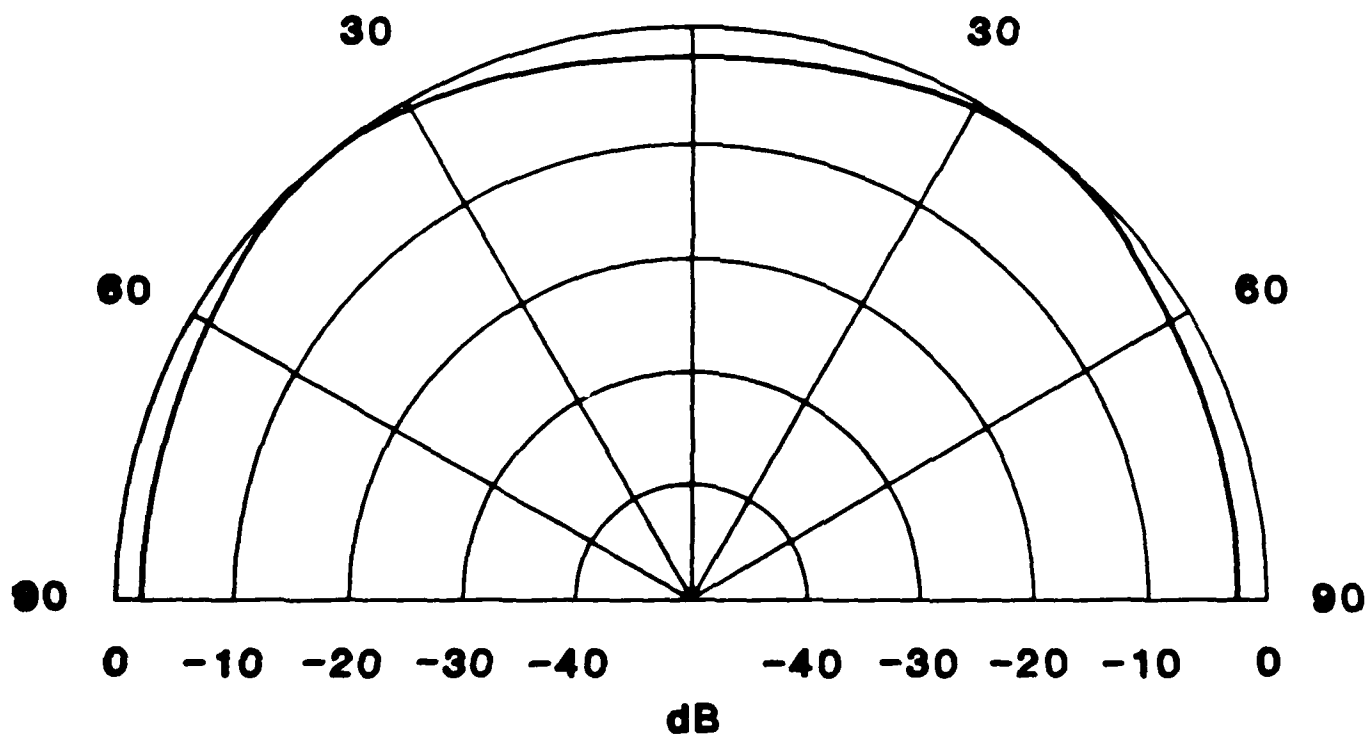
θ

Figure 8b

$\overline{E}$-PLANE PATTERN

$\epsilon_1 = 1.3 \qquad \dfrac{n_1 B}{\lambda_o} = 1.041$

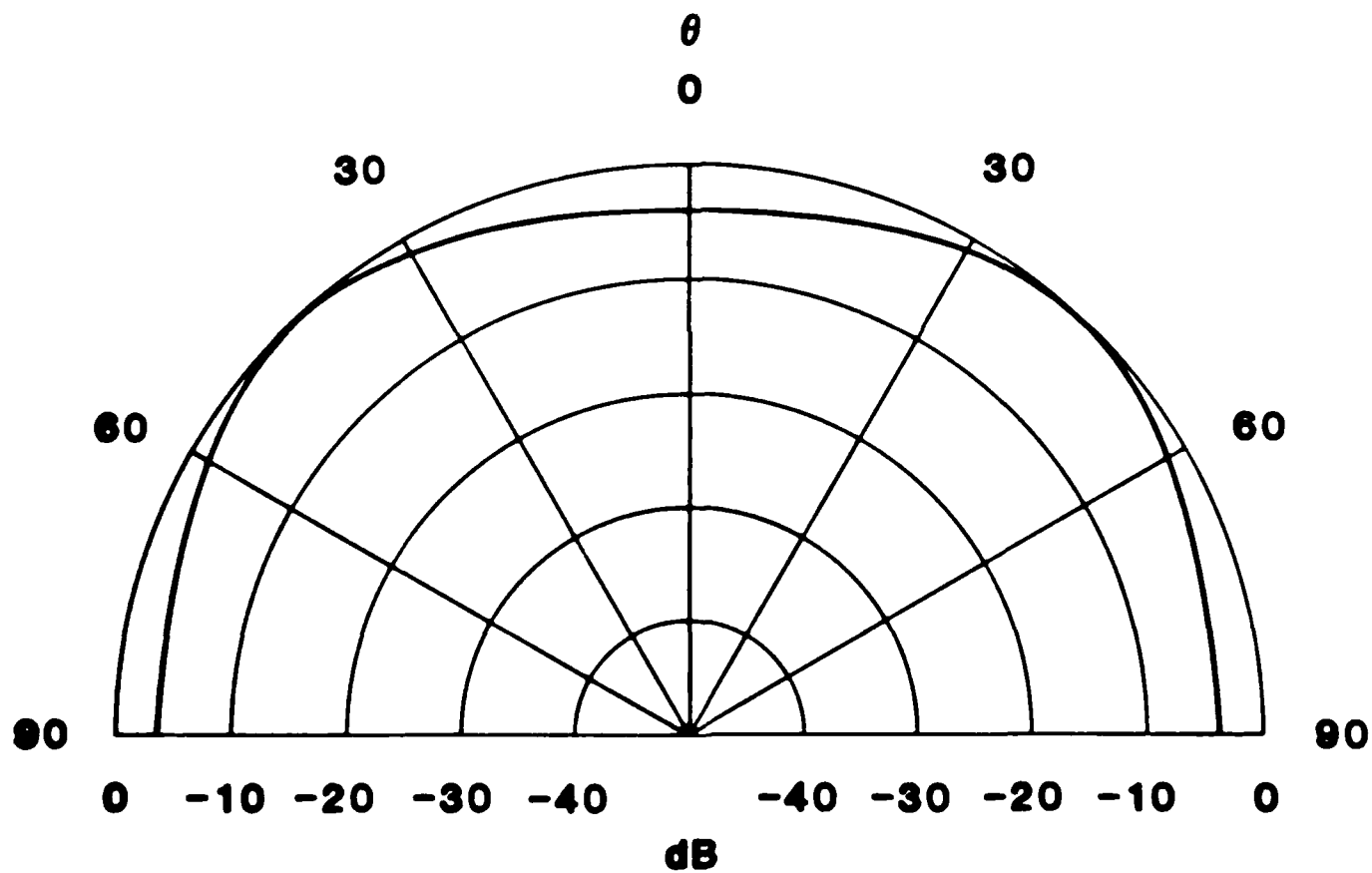$\mu_1 = 1.0 \qquad \dfrac{n_1 Z_o}{\lambda_o} = .424$

Figure 8c

Ē-PLANE PATTERN

$$\epsilon_1 = 1.1 \qquad \frac{n_1 B}{\lambda_o} = 1.658$$
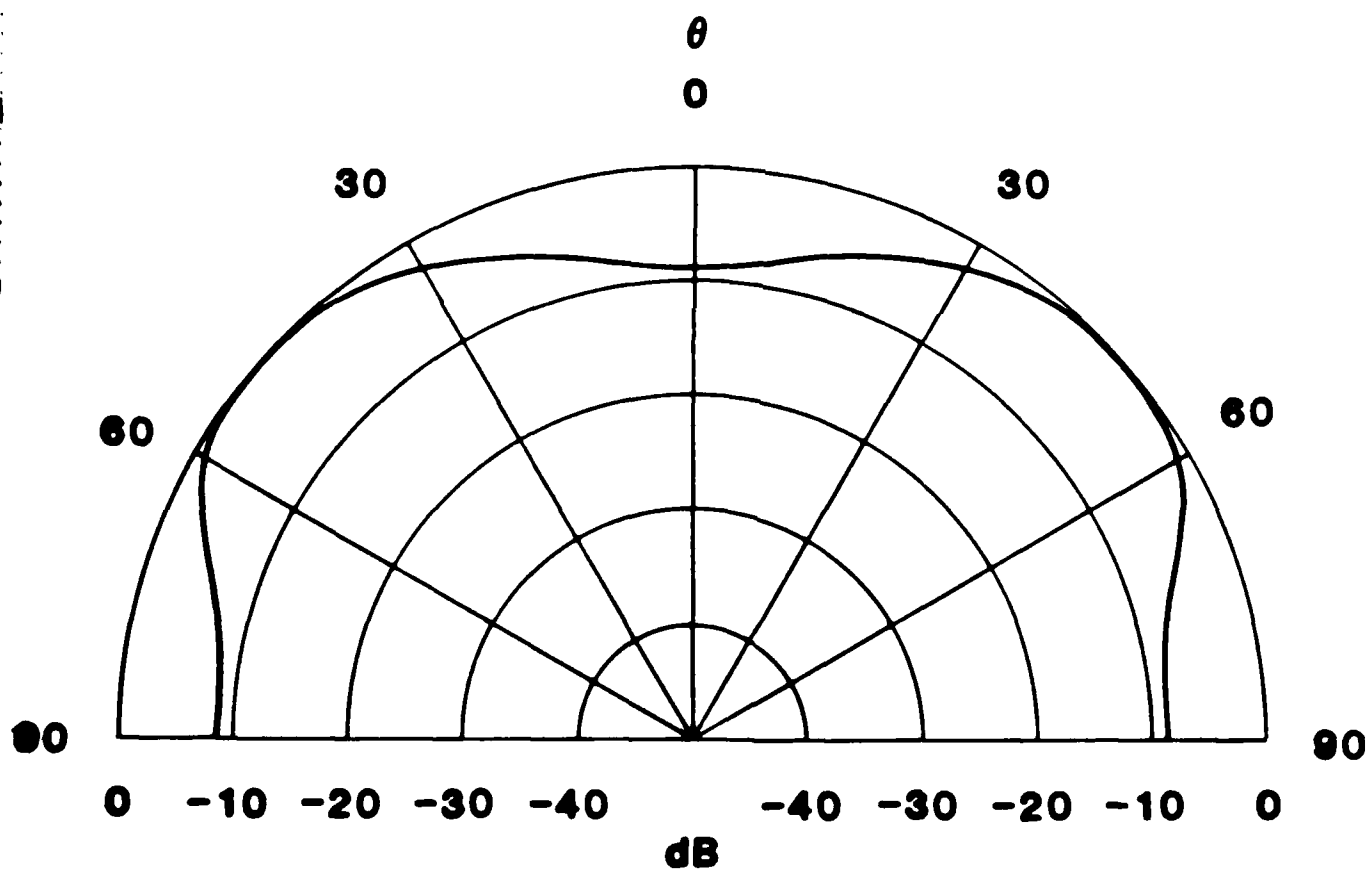
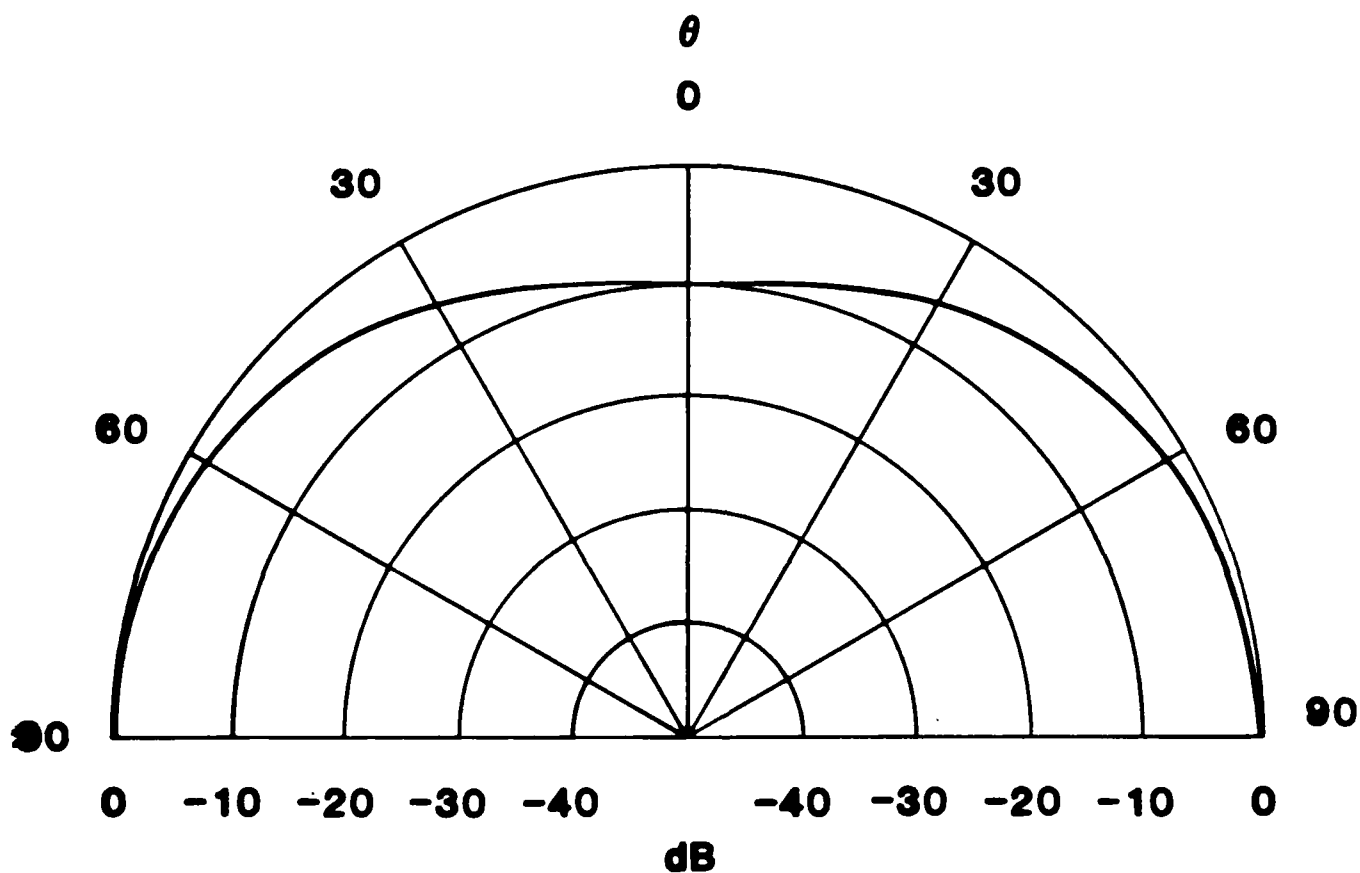$$\mu_1 = 1.0 \qquad \frac{n_1 Z_o}{\lambda_o} = .464$$

Figure 8d

Figure 9a

$\overline{E}$-PLANE 10dB Suppressed Pattern at $\theta = 0°$

$\epsilon_1 = 4.0$, $\mu_1 = 1.0$, $n_1 B/\lambda_0 = 0.580$, $n_1 z_0/\lambda_0 = 0.480$
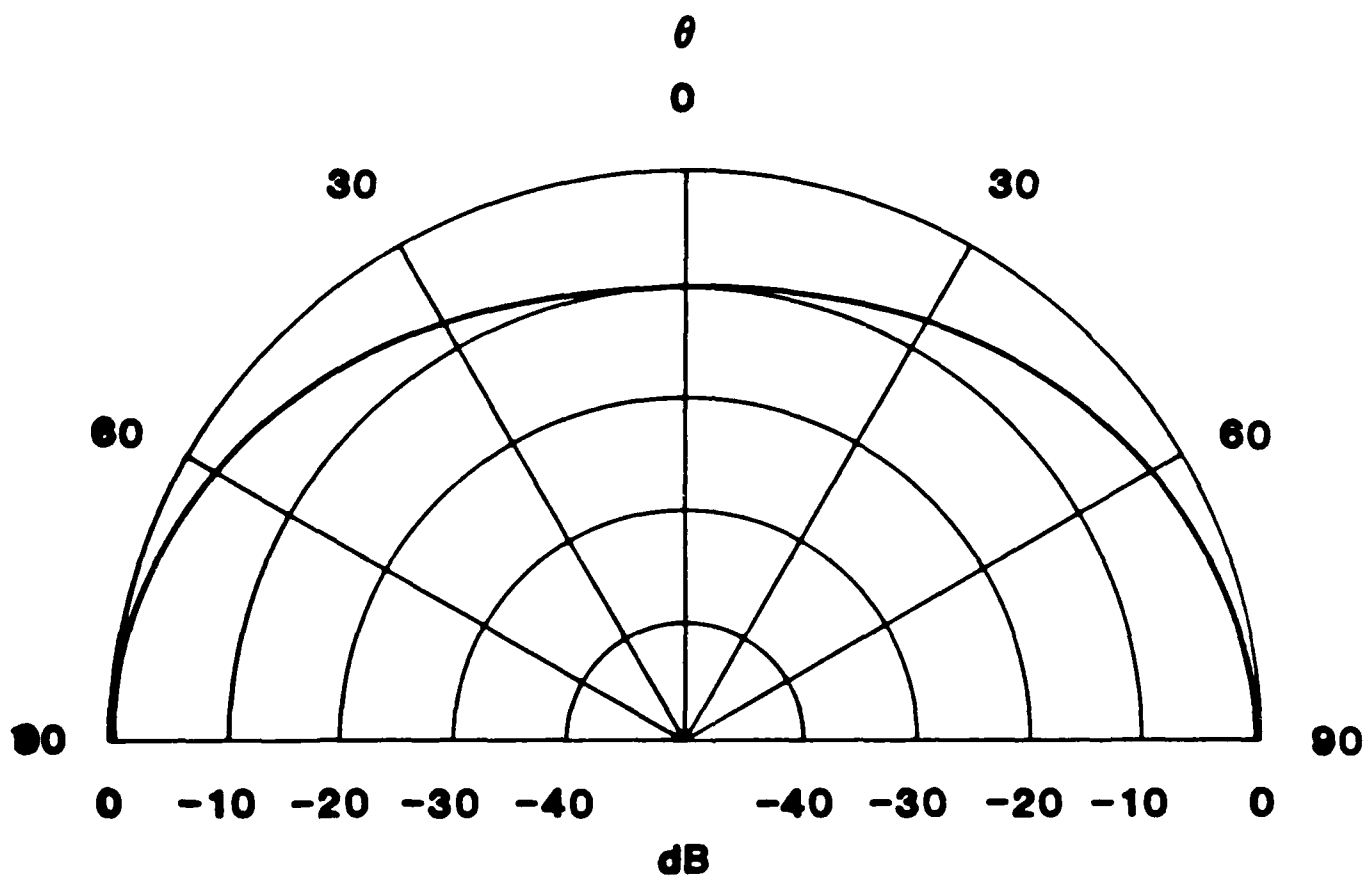
(Peak Gain is 6.753 dB at $\theta = \pi/2$)

Figure 9b

$\overline{H}$-PLANE 10dB Suppressed Pattern at $\theta = 0^\circ$

$\epsilon_1 = 4.0$, $\mu_1 = 1.0$, $n_1 B/\lambda_o = 0.865$, $n_1 z_o/\lambda_o = 0.450$

(Peak Gain is 7.665 dB at $\theta = \pi/2$)

FILM

Figure 7b

$$\frac{n_1B}{\lambda_o} \text{ vs. } \epsilon_2 \text{ for } \overline{H}\text{-PLANE}$$

.05

1   5   10

ϵ_2

$$\frac{n_1B}{\lambda_o} \text{ vs. } \epsilon_2 \text{ for } \overline{H}\text{-PLANE}$$